UNIVERSIDADE DE LISBOA

FACULDADE DE CIÊNCIAS

DEPARTAMENTO DE ENGENHARIA GEOGRÁFICA, GEOFÍSICA E ENERGIA

Deterministic Tsunami Hazard Assessment of Sines - Portugal

Mestrado em Ciências Geofísicas
Oceanografia

Martin Wronna

Dissertação orientada por:
Prof. Doutor Jorge Miguel Alberto de Miranda, Profª Doutora Maria Ana de Carvalho Viana Baptista

2015

Abstract

This study employs a deterministic approach for multiple source tsunami hazard assessment for the city and harbour of Sines – Portugal, one the test-sites of project ASTARTE. Sines holds one of the most important deep-water ports which contains oil-bearing, petrochemical, liquid bulk, coal and container terminals. The port and its industrial infrastructures are facing the ocean southwest towards the main seismogenic sources. This work considers two different seismic zones: the Southwest Iberian Margin and the Gloria Fault. Within these two regions, we selected a total of six scenarios to assess the tsunami impact at the test site. The deterministic approach consists in solving linear and non-linear shallow water equations using an explicit leap-frog scheme to obtain water elevations in predefined grids for a defined time step. Numerical model computation process is launched after defining an initial seafloor displacement on a prepared set of nested grids. The Digital Elevation Model includes bathymetric and topographic information with 10m resolution in the study area. To do the tsunami simulations a Non-linear Shallow Water Model With Nested Grids – NSWING is used. In this study, the static effect of tides is analysed for three different tidal stages. Tsunami impact scenarios are described in terms of inundation area, maximum values of wave height, flow depth, drawback, run-up and inundation distance. Synthetic waveforms are computed for virtual tide gauges at specific locations outside and inside the harbour. The final results describe the impact at Sines test site considering the different source scenarios at mean sea level, the aggregate scenario and the influence of the tide on the aggregate scenario. The results confirm the composite source Horseshoe and Marques Pombal fault as the worst case tsunami scenario. It governs the aggregate scenario with about 60% and inundates an area of 3.5km².

Key-words: Deterministic tsunami hazard assessment, numerical modelling, aggregate scenarios, integrated hazard maps.

Resumo

Neste trabalho apresenta-se uma abordagem determinística de perigo de tsunamis considerando múltiplas fontes para a cidade costeira de Sines, Portugal. Tsunamis ou maremotos são eventos extremos, energeticamente elevados mas pouco frequentes. Normalmente são geradas por um deslocamento duma grande quantidade de água seja por erupções volcánicas, collapse de caldeiras, deslizamentos de massa, meteorites ou terramotos submarinos. A grande maioria é causado pelos terramotos submarinos. Neste trabalho estuda-se sómente efeitos causado por tsunamis gerados pelos deslocamentos de solo submarino devido a terramotos. O evento no oceano Índico em 2004 demonstrou a necessidade de um sistema de alerta operacional global. E o Tohoku terramoto em 2011 moustrou as limitações do conhecimento científico respetivamente às zonas fontes, os impactos costeiros e medidas de mitigação. A partir desta data na zona Noreste Atlantico e Mediterrâneo e mares adjacentes (NEAM) esforços foram feitos para melhorar as capacidades de avaliação de perigo de tsunamis. Em Portugal a zona considerada mais ativa é o Golfo de Cadiz. Relatos históricos antigos voltam atrás até 60 BC, mas evidências geológicas mostram eventos energeticamente elevadas até 218 BC.

A costa portuguesa é altamente exposta ao perigo de um tsunami a partir de fontes tectónicas ativas locais e regionais. A zona principal tsunamigenica é o SWIM (Margem sudoeste da Península Ibérica), que inclui numerosas falhas inversas que mergulham em direcção sudeste. O evento mais rigoroso foi o 1º Novembro 1755 causado pelo famoso terramoto de Lisboa com mais do que dez mil vítimas mortais e uma magnitude estimada de 8.5. A fonte do tsunami ainda não é conhecida definitivamente, pois na altura ainda não havia instrumentos para registrar sismos. A fonte foi aproximada por diferentes autores utilizando as informações históricos e assuma-se que é localizada na zona SWIM. O impacto do tsunami ocorreu na bacia inteira do ocenao Atlântico Norte com maior impacto na Ibéria e em Moroccos. No seculo 20 no dia 28 de Fevereiro 1969 um sismo de magnitude 7.9 causou um tsunami pequeno com uma amplitude de 0.5m em Lagos e Cascais. As ondas aproximaram-se da costa por volta das 3 de manha em condições maré vazia e não causaram danos significativos.

O trabalho foi desenvolvido no ambito do projeto ASTARTE [Grant 603839]. Em Sines encontra-se um dos portos mais importantes de agua profunda de Portugal contenido terminais petrolíferos, petroquímicos, graneis líquidos, carvão e contentores. O porto está ligado aos centros industriais em Sines com infraestruturas frageis como gasoduto, oleodutos, tanques de gás natural liquefeito ou cinturões industriais, quais ocorrem o risco de ser danificados. Possiveis danos geram riscos addicionais como explusões ou poluições ambientais. Na zona sul da area do estudo encontra-se o central thermoeletrico da EDP que utliza a água do mar pelo arrefecimento dos geradores. Sines também e um destino turístico com um porto de recreio e com varias praias associadas aos desportos náuticos como a pesca deportiva, a vela, o mergulho e o surf. A zona de estudo inclui o porto de recreio e as praias de Vasco da Gama e de São Torpes. O porto, o central thermoelétrico e as suas infrastruturas industriais e as praias enfrentam ao Atlantico a sudoeste direcionado às zonas principais de rupturas sísmicas consideradas suficientemente fortes de causar tsunamis e por causa disso a zona de estudo escolhido é altamente exposto ao perigo dum tsunami. Foram consideradas as zonas de fontes a falha da Gloria (GF) e a zona da margem sudoeste da península Ibérica (SWIM) e cinco falhas diferentes, nomeadamentes: A falha da Gloria que é uma falha de cisalhamento que defina a fronteira entre Eurasia e Nubia; a falha de Cadiz Wedge (CWF) que é considerada como uma zona de subducção e as falhas do banco de Gorringe (GBF), de Ferradura (HSF) e de Marques Pombal (MPF) que são falhas inversas que mergulham em direcção sudeste. Adicionalmente foi considerado uma combinação da falha de ferradura e da falha Marques Pombal (HSMPF) para a simulação. Um ruptura simultânea de falhas com parâmetros parecidos foi proposta por varios autores como uma possível fonte do tsunami em 1755. A zona SWIM é considerado uma zona complexa em termos geodinâmicos onde varios processos atuam simultaneamente. Para cada falha identificada e para a combinação HSMPF o pior dos cenários sísmicos foi assumido para o procedimento da modelação numérica.

A abordagem deterministica consiste em resolver as equações lineares e não-lineares de água pouca profunda para puder obter as elevações da superfície livre do oceano em cada passo tempo definido. As equações de água pouca profunda são válidas devido do facto que tsunamis são ondas longas. Ondas são consideradas longas quando o seu comprimento de onda λ é muito maior que a altura de coluna de agua h ou quando se verifica $\frac{h}{L} < \frac{1}{25}$ (Intergovernmental Oceanographic Commission, 2013).

Na simulação numérica da propagação do tsunami é utilizado modelo NSWING (Non-linear Shallow Water Model with Nested Grids) (Miranda et al., 2014) que resolve as equações de água pouca profunda utilizando um esquema "leap-frog" explícito para os termos lineares e um esquema "upwind" para os termos não-lineares. Após definir o deslocamento inicial do fundo do oceano o modelo calcula as soluções para cada cenário dentro de um sistema de grelhas encastradas. Para poder calcular os deslocamentos iniciais aplicando a teoria de inelasticidade de Okada (1985) foram utilizados parâmetros presentados de campanhas e estudos recentes. Foi aplicado uma distribuição dum slip não uniforme onde o slip defina o deslocamento inicial em cada célula da grelha. Este deslocamento inicial e traduzida pela superfície livre onde o processo numérico da propagação do modelo começa e as equações de água pouca profunda são resolvidas em cada passo tempo para cada célula de sistema de grelhas ligadas. Neste estudo o sistema das grelhas encastradas ou "nested grids" consiste num conjunto de quatro grelhas ligadas. Na zona fonte e em oceano aberto utiliza-se uma grelha com células maiores. Células de 640x640m reduzindo-as para 10x10m quando se atinge a zona de estudo. Usam-se duas grelhas intermédias 160m e 40m aplicando um fator de refinamento de 4. Para puder analisar efeitos locais com essa resolução alta precisa-se um DEM (modelo digital de terreno) com informações detalhadas sobre a bathimetria e a topografia da area de estudo. O DEM foi elaborado utilzando um conjunto de dados do Instituto Hidrográfico de Portugal e da Direção-geral do Território num SIG (sistema de informação geográfica). A inundação é obtida a partir dum algoritmo designado "moving boundary-percurso da linha de costa" baseado em células secas e células inundadas para conseguir seguir a linha da costa (Liu et al., 1995).

Também foi considerado o efeito da maré. Os valores de maré cheiá foram obtidos calculando a média das médias de todas as Preias-mar e da maré vazia a média das médias de todas as Baixas-mar de 2012 até 2014. Para cada cenário foram calculadas três condições de maré, da condição maré cheia, do nivel médio do mar e da condição maré vazia.

Os resultados finais são apresentados em forma de mapas integrados de perigo para cada cenário considerado e para o cenário agregado. Cada mapa integrada de perigo consiste em valores máximos de altura de onda (MWH), profundidade de fluxo (MFD), recuo (MDB), runup (MRU) e distância de inundação do cenário correspondente. Formas de ondas sintéticas foram calculadas em pontos da grelha designados por marégrafos virtuais em pontos representativos dentro e fora do porto. Os resultados finais descrevem o impacto em Sines considerando cada único cenário de nível médio do mar, o cenário agregado e a influência da maré no cenário agregado. Os resultados confirmam que o pior caso cenário é a combinação da falha de ferradura e da falha Marques Pombal HSMPF. Este cenário domina o cenário agregado com aproximadamente 60% e inunda uma área de 3.5km².

Palavras-chave: Abordagem determinística do perigo de tsunami, modelação numérica, cenários agregados, mapas de perigo integrados.

Acknowledgements

I would like to thank Maria Ana Baptista, Jorge Miguel Miranda and Rachid Omira for their great support and fruitful discussions throughout the entire investigation process, Carlos Antunes for providing the GPS RTK equipment of Lisbon Faculty of Sciences, Commandant José Brazuna Fontes of Sines harbour for his support for the field survey and Direção Geral do Território for making available LIDAR data of the study area.

I wish to express my thanks to my family for their support, especially my parents Ursula and Günter Wronna, my sister Edith Wronna, my Grandmother Christine Achleitner and my aunt Gertrude Kneissl. And I wish to express my gratefulness to my girlfriend Maria Fuchs for her patience and mental motivation. Additionally I want to thank my friends Daniela, Joana, Laura, Susana, Alessandro, Carlos and Miguel who supported me throughout the master classes.

Index

List of figures

List of tables

1. Introduction

Tsunamis are low frequency but high impact hazards for coastal societies. Tsunamis are sets of waves produced by an abrupt displacement of a large amount of water. Generating processes are usually geologic activities such as earthquakes, volcanic eruption or landslides. Rare meteorite impacts extreme meteorological events for example abrupt atmospheric pressure jumps may also cause Tsunamis. The term tsunami originates from the Japanese "tsu" what means harbour and "nami" what means wave. Fisherman used it to describe flooding waves that sometimes destroyed the harbours. Submarine earthquakes trigger the great majority of tsunamis. Also from distant sources their impact can be tremendous. But not all submarine earthquake cause tsunamis only those that produce sufficient vertical seafloor deformation and dislocate the entire water column above. To prepare and protect coastal societies it is fundamental to understand better their impact at coastal shorelines. To understand better their nature scientists run numerical models to take precautions.

Basic terms and physical quantities used in the thesis are presented in table 1.1. Some physical quantities mentioned are depicted in Fig. 1.1.

Table 1.1 Basic terms and definitions used in this thesis.

Amplitude:	Height of the crest of the tsunami above mean sea level.
Bathymetry:	The measurement of the depth of the ocean floor from the water surface.
Topography:	The measurement of the elevation of the land surface from the sea level.
Wave Height:	The wave height is measured as the difference between wave crest and trough in a certain point.
Flow Depth or Inundation Depth:	Depth or height of the tsunami above the ground in the inundation zone. It measures the thickness of the water layer on land.
Inundation or inundation distance:	The horizontal distance in land that a tsunami penetrates; is measured perpendicular to the shoreline.
Maximum inundation area:	Maximum horizontal penetration of the tsunami inland
Mean Lower Low Water (MLLW):	The average of all the lower low water heights over a specific period.
Mean Sea Level (MSL):	The MSL is given by the arithmetic mean of hourly heights of tide height on the open coast or in adjacent waters which have free access to the sea, observed over a specific time period. The MSL is often used as geodetic datum.
Mean Higher High Water (MHHW):	The average of all the higher high water heights over a specific period.
Maximum Drawback:	The maximum drawback gives the maximum area that remains dry offshore as the result of the tsunami arrival in the test site.
Run Up:	The maximum water elevation within the limit of inundation; this is usually greater than the wave amplitude at the coast. The run up height (or the elevation reached by the seawater) is measured relative to some given reference datum. In most studies and is referenced to MSL. In this thesis Run Up is referenced to MLLW, MSL or MHHW depending on the tide considered.
Period:	Time interval between two consecutive wave crests or troughs.
Recurrence or Return Period:	An interval of time long enough to encompass many events divided by the number of events equal or greater than a specific magnitude that are expected to occur.
Tsunami Travel Time:	Time required for the first tsunami wave to propagate from its source to a given point on a coastline.
Tsunamigenic:	Capable of producing a tsunami.

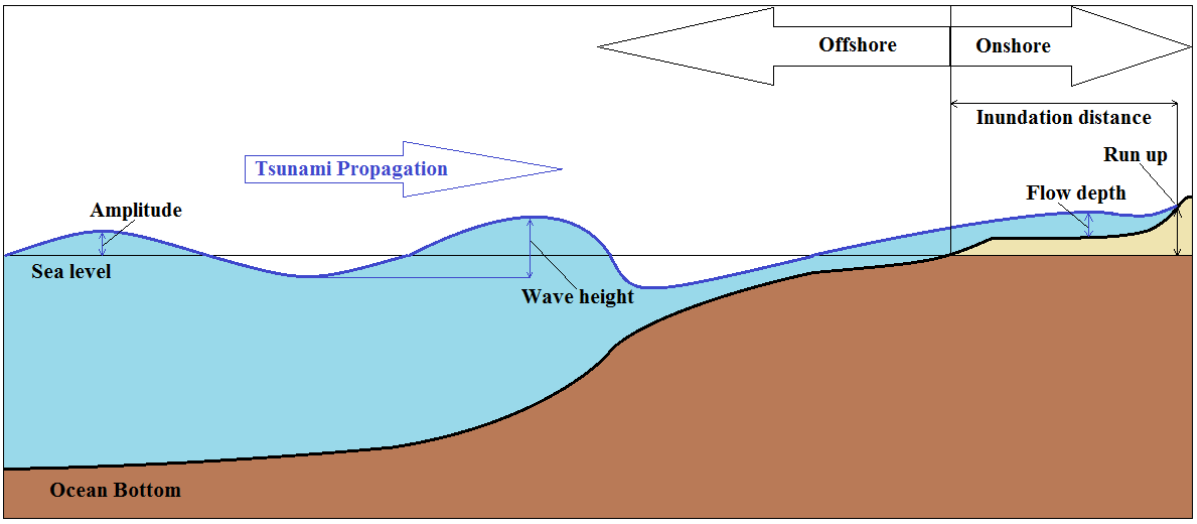

Figure 1.1 Schematic illustration of physical quantities such as amplitude, wave height, flow depth, run up and inundation distance referenced to a given sea level.

The 26th December, 2004 Indian Ocean and the 11th March, 2011 Tohoku-Oki striking tsunami events raised awareness due to the enormous loss of life and property. The Indian Ocean event in 2004 demonstrated the need for operational early warning systems around the world. However, seven years later, the 2011 Tohoku-Oki event showed the limitations of the scientific knowledge concerning tsunami sources, coastal impacts, and mitigation measures. Since then, in the NEAM region (North East Atlantic, Mediterranean and connected seas) many efforts have been addressed to understand better the tsunamigenic sources and to improve the tsunami hazard assessment capabilities. Within the NEAM region, the Gulf of Cadiz is among the most tsunami hazardous areas. The historical reports include events dated back to 60 BC (Mendonça, 1758, Baptista and Miranda, 2009; Kaabouben et al., 2009). However, the geological evidence indicates that high energy events occurred back to 218 BC (Luque et al., 2001).

This study was developed in the framework of ASTARTE project "Assessment, STrategy And Risk Reduction for Tsunamis in Europe" [Grant 603839]. The project uses nine test sites in the North East Atlantic and Mediterranean (NEAM) Region. The test site selection considered that:

- Test sites can be impacted by regional and local tsunami sources, which put different levels of stress on detection and forecasting
- Different tsunami source types, such as earthquakes, landslides, volcanoes and rockslides, some of which not included in NEAMTWS
- Different values at risk including industry, harbours and other infrastructures, and ecosystems
- Different coastal communities such as fishing communities, coastal cities and tourist developments
- Test sites include a broad geographical coverage, in both North-east Atlantic and Mediterranean coasts

In Portugal the test site is the city of Sines. The study area consists of different topographic features like beaches, rocks, rocky outcrops, plains and smaller river course valleys and is interfered by big harbour and industrial structures.

The Portuguese coast is exposed to tsunami threat from local and regional tectonic sources (Intergovernmental Oceanographic Commission, 2013). The main tsunamigenic area is the SWIM (South West Iberian Margin), with some considerable SE dipping inverse faults (Zitellini et al., 2009, Matias et al., 2013). The most severe tsunami occurred on November 1st 1755. The tsunami followed the Lisbon earthquake with an estimated magnitude of 8.5 by Martins and Mendes Victor (1990). The event caused more than 900 casualties exclusively due to the tsunami (Baptista et al., 1998a). This

magnitude was more recently re-evaluated by Solares and Arroyo (2004) with an estimate of 8.5±0.3. The tsunami hit the entire northern Atlantic basin with huge impact in Iberia and Morocco (Baptista and Miranda, 2009). In the 20th century, the February 28th, 1969 earthquake with a magnitude of 7.9 (Fukao, 1973) caused a small tsunami of 0.5 m amplitude in Lagos and Cascais (Baptista et al., 1992; Baptista and Miranda, 2009). The tsunami waves hit the coast in low tide conditions at circa 3 a.m. (Baptista et al., 1992) and no significant damage was observed.

The second tsunamigenic zone to be considered is the Gloria Fault. The Gloria fault is a segment of the Eurasia-Nubia plate boundary. It is a large strike slip fault, located between 24ºW and 19ºW, with scarce seismic activity. Nonetheless, this area was the location of several large events during the 20th Century, in particular the November 25th, 1941 earthquake, a submarine strike-slip event of magnitude 8.3-8.4 (Gutenberg and Richter, 1949) and the May 26th, 1975 with magnitude 7.9 (Lynnes and Ruff, 1985; Grimson and Chen, 1986).

In recent years, a considerable number of tsunami hazard assessment studies were published for the North East Atlantic area. Most studies focus on the tsunami impact in the Gulf of Cadiz using a scenario based or deterministic approach, namely: Lima et al. (2010), Omira et al. (2010), Omira et al. (2011), Atillah et al. (2011), Baptista et al. (2011a), Renou et al. (2011), Omira et al. (2013), Benchekroun et al. (2013) and Lemos et al. (2014).

Actually, two different assessment methods are used to study the tsunami impact at a certain test site, the PTHA (Probabilistic Tsunami Hazard Assessment) and DTHA or SBTHA (Deterministic Tsunami Hazard Assessment or Scenario Based Tsunami Hazard Assessment).

The PTHA approach consists in considering the recurrence rates of earthquake scenarios with different magnitudes. By knowing the recurrence rates of the different magnitude scenarios a database is generated using numerical modelling methods. Apart from this results a probability exceeding a certain wave height/flow depth in a given period is assessed. Recently, Omira et al. (2015) published a probabilistic tsunami hazard assessment for the North East Atlantic. These studies gain in reliability the longer the geological databases reach back. Another method used in PTHA is to apply an aleatory statistical tool called Monte Carlo simulations (e.g. Ten Brink et al., 2009, Grilli et al., 2009, Sørenson et al., 2012).

The DTHA or SBTHA methodology consists of studying the impact of specific tsunami events – tsunami scenarios - in the study area. Usually the specific tsunami events are based on geological information considering the Maximum Credible Earthquake (MCE) scenario or the Worst-case Credible Tsunami Scenarios (WCTS) considering the typical fault (TFs) of the source zones in the study area. Numerical simulation of the chosen scenarios calculates the tsunami impact in the test-site. By estimating parameters as wave height, flow depth, drawback, inundation distance hazard maps are elaborated. This methodology has been applied to assess tsunami hazard around the globe (e.g. Baptista et al., 2011a, Tonini et al., 2011, Mitsoudis et al., 2012, Phuong et al., 2014, Wijetunge, 2014). The deterministic approach is more suitable to establish tsunami mitigation measures and coastal municipality authorities.

In this master thesis, the DTHA approach has been used to evaluate the tsunami impact in Sines. The impact is described in terms of maximum wave height (MWH), maximum flow depth (MFD), maximum run up (MRU) and maximum drawback (MDB). Further the aggregate scenario has been built plotting the MWH in each cell considering the contribution of the individual scenarios (Tinti et al., 2011).The study area contains the country's most important deep water port that is connected to big industrial complexes by fragile infrastructure such as pipelines and conveyor belts. In summer the city is a popular tourist destination.

The final results are presented in integrated hazard maps for all the considered and the aggregate scenario. Each integrated hazard map consists of MWH, MFD, MRU and MDB of the corresponding scenario. The analysis of tide effect consists of three different tidal stages mean lower low water (MLLW), mean sea level (MSL), and mean higher high water (MHHW). Further the contribution of each scenario to the aggregate tsunami impact is presented at MSL condition.

1.1. Wave and Tsunami physics

In this master thesis the focus has been laid on studying the hazard of earthquake generated tsunamis. Most tsunamis are triggered by submarine earthquakes. But not all submarine earthquakes cause tsunamis just those that cause predominantly large vertical deformation of the seafloor (Synolakis, 2003). These earthquakes are usually stronger than magnitude 7.0 and occur typically in between 0 and 40 km depth (Bryant, 2014). The theoretical introduction to the linear theory that yields the most important properties for surface gravity waves is based on Sorensen (2006).

A surface gravity wave is when a resting water surface is disturbed in vertical direction and gravity acts to return the displaced water mass back to equilibrium. Because of inertia the returning mass of water passes the equilibrium position and causes an oscillating movement of the surface. This movement affects the adjacent water surface, thus wave propagation is initiated. This mechanism moves energy from one location to another at water surface with almost no net displacement of the fluid itself (Sorensen, 2006).

Wind induced gravity waves just affect the sea surface and water particles rotation and transported energy decreases in depth. They have typical periods between 1 to 25 seconds which corresponds to tens up to a few hundreds of metres wave length (Bryant, 2014).

Tsunami are also gravity waves as huge mass of water is displaced vertically. Because of that their periods are commonly between 100 and 2000 seconds. Typical wavelengths of tsunamis are from 10 to 500 km (Bryant 2014). The existence of a tsunami can be divided in three stages.

1.) Generation: Tsunamis are triggered by an immediate displacement of the entire water column, caused by earthquakes, volcanic eruptions, landslides or rare impacts of cosmic objects.

2.) Propagation in the deep Ocean: Starts when gravity is acting to restore equilibrium in the dislocated water column.

3.) Near shore propagation and inundation: Because of shallower bathymetry the approaching tsunami is strongly deformed and shoaling forces the wave to pile up. As periods are long and water masses cannot escape back to the ocean, water pushes landwards and causes inundation.

Tsunamis behave the most time as shallow water waves and their particles move on elliptic tracks in the entire water column, so transferred energy is not decreasing in depth.

Generally Ocean waves on the surface depend on three physical factors. (1) Gravitation acting to re-establish the equilibrium of the free surface, (2) Surface tension, as pressure varies underneath a wave and (3) Viscosity that handles dissipation of energy.

Apart from the linear wave theory, first introduced by Airy in 1845 several important properties of surface gravity waves can be derived. The linear wave theory represented in this study is based on following assumptions:

- Water is considered as a homogeneous, incompressible fluid and, as the studied wavelength is long enough (greater than approx. 3cm) that surface tension can be neglected.
- The flow is irrotational $\nabla \times \vec{v} = 0$, so there is no shear stress at the surface at the air-sea boundary and water slips without friction over a solid bottom. The bottom is impermeable and horizontal, thus water depth d is considered constant. Thus there is no loss energy due to sloping bottom. The linear wave theory uses a velocity potential ϕ to describe the motion on the fluid surface, $\vec{v} = -\nabla\phi$. Accepting the irrotational movement, $-(\nabla \times \nabla\phi) = 0$, the flow is non-divergent and the velocity potential ϕ must satisfy Laplace's equation.

$$\nabla^2\phi = \frac{\partial^2\phi}{\partial x^2} + \frac{\partial^2\phi}{\partial z^2} = 0 \tag{1.1}$$

where x represents the horizontal and z the vertical coordinate.

- The pressure on the surface is assumed to be constant, thus atmospheric pressure gradient is zero, and pressure difference between wave crest and trough is negligible.

These approximations are valid if the wave height is small compared to the wave length and water depth. Thus water particle velocities (proportional to the wave height) are small compared to the phase velocity (related to the wave length and water depth).

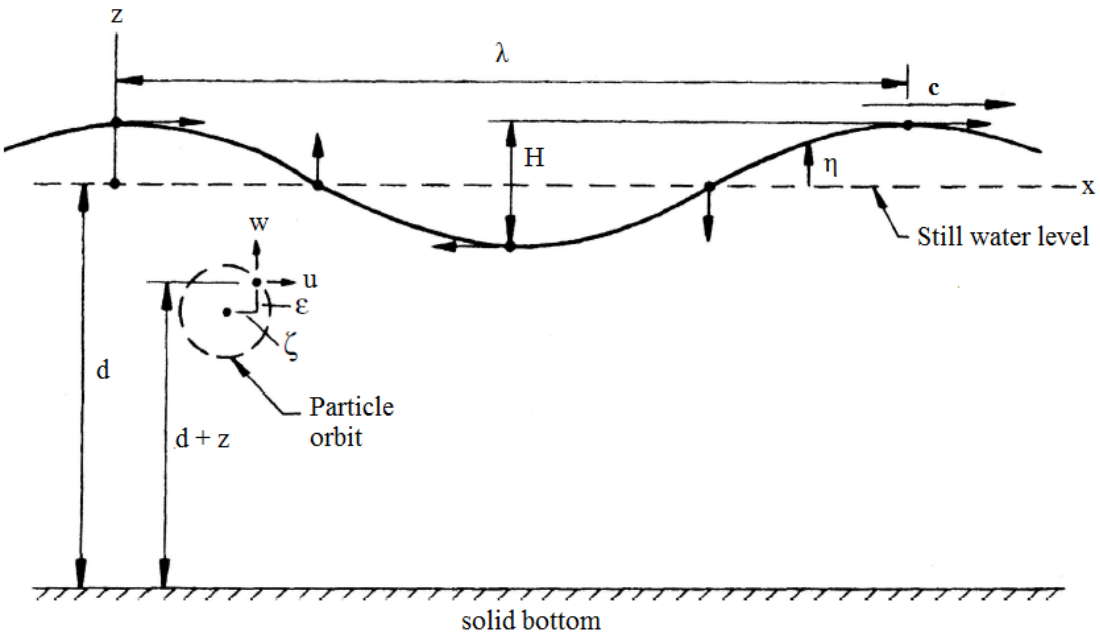

Figure 1.2 Schematic sketch of the simplified conditions of waves propagating in x-direction; modified from Sorensen (2006).

Figure 1.2 shows a wave traveling in x-direction with the phase velocity c upon the stated assumptions in a x, z coordinate system. The x-axis corresponds to the still water level. Water depth is d and at the solid bottom $d = -z$. The wave height is H defined as the difference between wave crest and wave trough and the amplitude A is $A = \frac{H}{2}$. The water surface is given by $z = \eta$ where η is a function of x and time t, $\eta(x, t)$. The wave length λ is given by the distance between two consecutive wave crests. The wave travels the distance λ in the period T, thus the phase velocity is given by

$$c = \frac{\lambda}{T} \tag{1.2}$$

The arrows along the water surface indicate particles movement when a wave crest or trough is passing indicating a clockwise movement. When a wave is travelling under deep water conditions the particles movement is nearly circular and diminishes in depth. In shallow water conditions the particles tracks are elliptical and reach the bottom. The horizontal and vertical components of the particles movement are u and w respectively and the position is given by ζ and ε coordinates at any instant. ζ and ε are referenced to the centre of the particles track.

Important dimensionless parameters are:

$$k = \frac{2\pi}{\lambda}, \tag{1.3}$$

where k is the wave number and

$$\sigma = \frac{2\pi}{T}, \tag{1.4}$$

where σ is the angular frequency.

The linear theory was developed by solving Laplace's equation given in (1.1), applying certain boundary conditions. At the ocean bottom the kinematic boundary condition as there is no vertical flow across the boundary, is

$$w = \frac{\partial \varepsilon}{\partial t} = \frac{\partial \phi}{\partial z} = 0, \text{at } z = -d \tag{1.5}$$

Where w describes the velocity of the vertical flow, ε is the vertical coordinate for water particle at any instant and ϕ is the velocity potential. And the kinematic boundary condition at the surface establishes the relation between the vertical movement of the particle at the surface, to the surface position.

$$w = \frac{\partial \phi}{\partial z} = \frac{\partial \eta}{\partial t} + u\frac{\partial \eta}{\partial x}, \text{ at } z = \eta \tag{1.6}$$

The Bernoulli equation for an unsteady irrotational flow is:

$$\frac{P}{\rho} + gz + \frac{\partial \phi}{\partial t} + \frac{1}{2}(u + w)^2 = 0 \tag{1.7}$$

where P is the pressure, ρ is the fluid density and g the acceleration of gravity ($g \approx 9.81 ms^{-2}$). At the surface pressure becomes zero and the dynamic boundary condition is given by

$$gz + \frac{\partial \phi}{\partial t} + \frac{1}{2}(u + w)^2 = 0, \text{ at } z = \eta \tag{1.8}$$

The kinematic and dynamic boundary condition are linearized using the still water surface yielding

$$w = \frac{\partial \eta}{\partial t}, \text{ at } z = 0 \tag{1.9}$$

and

$$g\eta + \frac{\partial \phi}{\partial t} = 0, \text{ at } z = 0 \tag{1.10}$$

To find the velocity potential that satisfies the Laplace's equation (1.1) at the established boundary conditions (1.9) and (1.10), the method of separation of variables assuming a trial solution the form $\phi(x, z, t) = X(x)Z(z)T(t)$ is used as shown in Pedlosky (2003). The solution for the velocity potential ϕ yields to a sinusoidal time dependent function.

$$\phi = \frac{Ag}{\sigma}\frac{\cosh k(d + z)}{\cosh kd}\sin(kx - \sigma t) \tag{1.11}$$

where A is the wave amplitude and σ is the angular frequency. By knowing wave height H, wave length λ and water depth d the wave can fully characterized. Applying equation (1.11), the linearized dynamic boundary condition the solution for the free surface $\eta(x, t)$ at $z = 0$ is given by

$$\eta(x, t) = \frac{1}{g}\left(\frac{\partial \phi}{\partial t}\right)_{z=0} = A\cos(kx - \sigma t) \tag{1.12}$$

Combination of the kinematic and dynamic surface boundary condition and eliminating $\eta(x,t)$ one gets:

$$\frac{\partial^2\phi}{\partial t^2} + g\frac{\partial\phi}{\partial z} = 0, \text{ at } z = 0 \tag{1.13}$$

By inserting the velocity potential given in (1.11), and differentiating and rearranging the harmonic time dependence of the velocity potential with the angular frequency of gravity waves σ is derived.

$$\sigma = \sqrt{gk\tanh kd} \tag{1.14}$$

The phase velocity c of gravity waves can be expressed in terms of wave number k and angular frequency σ using equations (1.3) and (1.4)

$$c = \frac{\sigma}{k} = \sqrt{\frac{g}{k}\tanh kd} \tag{1.15}$$

For waves propagating in deep water conditions, where $\frac{d}{\lambda} \geq \frac{1}{25}$ (Intergovernmental Oceanographic Commission, 2013) the term $\tanh kd$ in equation (1.15) tends towards 1, ($\tanh kd \approx 1$). Thus, in pure deep water conditions the phase velocity c for gravity waves yields

$$c = \sqrt{\frac{g}{k}} \tag{1.16}$$

In all physical problems regarding waves, dynamics involve a relationship between the wave number k and the angular frequency σ. This relationship can be expressed as

$$\sigma = \sigma(k) \tag{1.17}$$

This relationship is called dispersion relationship and is given in equation (1.14) for the linear wave theory. In case the angular frequency σ is a linear function of the wave number k, the phase velocity c is not depending on k. This waves are non-dispersive.

Most of the waves in oceans are dispersive and phase velocity c changes in respect with the angular frequency σ. That leads to deformation of the group of waves and individual phase amplitudes disappear when passing the group while propagation. The group velocity is thus expressed as variation of angular frequency σ in terms of wavenumber k.

$$c_g = \frac{d\sigma}{dk} \tag{1.18}$$

Differentiating and rearranging the group velocity c_g of gravity waves is given by

$$c_g = c\left[\frac{1}{2}\left(1 + \frac{2kd}{\sinh(2kd)}\right)\right] \tag{1.19}$$

For waves under deep water conditions wave number k is big, só $\sinh 2kd$ tends towards 0, ($\sinh 2kd \approx 0$). Thus

$$c_g = \frac{c}{2} \tag{1.20}$$

Waves in deep water are dispersive as their phase velocity c of the individual wave is travelling faster than the group. This leads to the deformation of the wave group.

Short waves approaching the shore line, enter gradually in shallower areas in a transition zone where they start to feel the ocean bottom. Within this transition zone the phase velocity c can be estimated with equation (1.15) which if k is expressed in terms of wave length λ turns into

$$c = \frac{\sigma\lambda}{2\pi} = \sqrt{\frac{g\lambda}{2\pi}\left[\tanh\left(\frac{2\pi d}{\lambda}\right)\right]} \tag{1.21}$$

And the group velocity c_g of water waves can be estimated by applying equation (1.19). Figure 1.3 depicts the transition zone where general approximations are not valid and full formulae from equations (1.15), (1.19) or (1.21) must be applied to obtain the correct velocities.

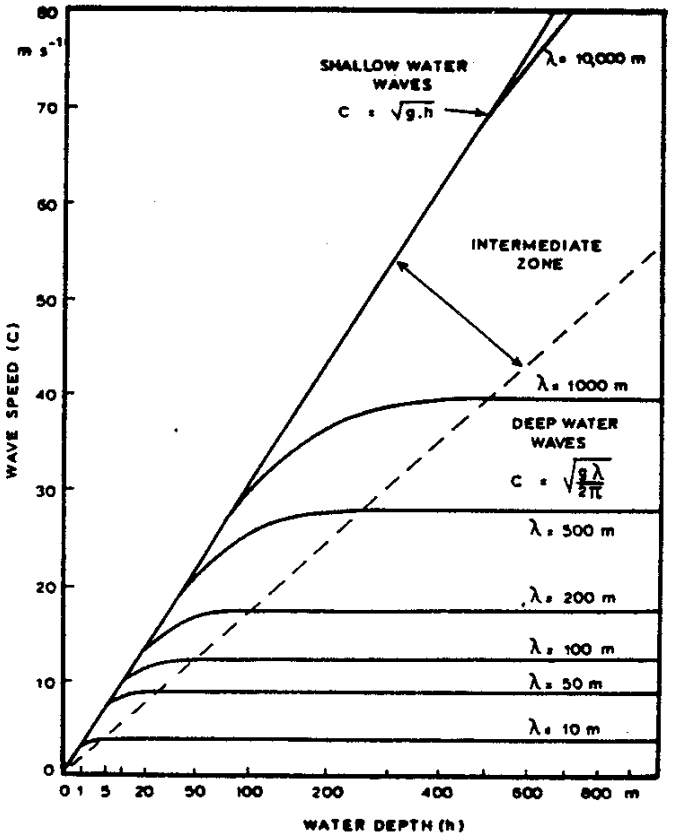

Figure 1.3 Illustration of wave condition depending on wave length and water depth (Bowden, 1983).

Tsunamis have great wave lengths and the relationship between the wave length λ and water depth d defines how gravity waves are classified. Most of the tsunamis travel under shallow water conditions. This is true if wave length λ is much larger than water depth d, $\frac{d}{\lambda} \leq \frac{1}{25}$ (Intergovernmental Oceanographic Commission, 2013). In shallow conditions hyperbolic tangent function of kd tends towards kd, ($\tanh kd = kd$), thus the waves phase velocity c is

$$c = \sqrt{gd} \tag{1.22}$$

The group velocity c_g of waves in shallow water conditions can be obtained from equation (1.19). Wave number k is low and $\sinh 2kd$ tends towards $2kd$. Thus, group velocity c_g yields

$$c_g = c = \sqrt{gd} \tag{1.23}$$

As group velocity and phase velocity are equal long waves in shallow water are considered as non-dispersive and their velocity depends only on the ocean depth. The phase velocity c and the group velocity c_g are equal for waves travelling in pure shallow water conditions. If the triggered gravity wave is long enough they travel as long waves in shallow water conditions. A wave travels purely under shallow water conditions if $d \leq \frac{\lambda}{25}$ (Intergovernmental Oceanographic Commission, 2013). In this case Equation (1.23) is valid and tsunamis travel dispersion less at speeds depending only on the oceans depth, if depth is constant. Considering an Ocean with 4000m depth the phase and group speed is approximately 700 km/h. When approaching shore areas ocean depth decreases and the waves slows down at a rate proportional to the square root of the ocean depth d (c.f. Equation (1.24). Due only little loss of energy whilst spreading throughout the oceans the waves pile up upon shoaling packing the entire energy into an even shallower water layer. The wave amplitude A increases at an inverse rate following the empirical Greens Law and can be applied on gradually sloping beaches in linear shallow water conditions (Helene & Yamashita, 2006).

$$A \propto \frac{1}{d^{1/4}} \tag{1.24}$$

where A is the wave amplitude and d is the ocean depth. Hence a 1m high wave when considering 2000m depth can get greater than 5m before landfall and still travel at speed of 35 km/h. Further due to their depth dependence the morphology of the bathymetry in shore areas can focus or defocus their transported energies. This fact may lead to different impact magnitudes within only few kilometres distance along the shoreline.

However, the linear wave theory serves to understand basically physical processes throughout a tsunami event and gives rapid and realistic wave height estimations near coastlines. Reality is more complex as the non-linear terms should be taken into account.

As already stated most tsunamis can be considered as long waves travelling in shallow water, the shallow water equations (SWEs) are commonly used to solve tsunami propagation problems. The initial sea surface deformation initiates wave propagation as the dislocated mass of water is regaining equilibrium due to gravity. The SWEs are obtained applying certain approximations to equations of the conservation of mass and conservation of momentum. The depth integrated form of the SWEs considers mean vertical velocities and acceleration. The linear form can be used as a first approximation considering propagation in deep ocean as the waves travel with a much smaller amplitude than ocean depth. However, when entering shallower water non-linear convective inertia forces and bottom friction become increasingly important and the non-linear SWEs must be applied. For transoceanic tsunamis the SWEs in spherical coordinates including the Coriolis Effect due to earth rotation should be considered. A more detailed view on the SWEs is presented in the methodology part in paragraph 2 about tsunami propagation.

1.2. Geoscientific context

In the morning of 1st November 1755 the big Lisbon earthquake followed by a tsunami destroyed the Portuguese capital and vast parts of the Portuguese, Spanish and Moroccan coastline. The shaking was felt all over Europe as far as Hamburg, the Azores and Cape Verde Islands, the strongest ones all over the Iberian Peninsula (Pereira de Sousa, 1919; Solares et al., 1979). The heaviest seismic shocks were felt from Cape St. Vincent (Pereira de Sousa, 1919). More than 500 aftershocks were reported lasting for more than nine months after the earthquake occurred (Mendes-Victor et al., 2008). As this was an historic event the magnitude could not be measured, but recent magnitude estimations are 8.5 ± 0.3 (Solares & Arroyo, 2004). The earthquake epicentre was located somewhere southwest of the

Portuguese coastline. The cataclysm was discussed intensely and theological theories were made. Kant and Voltaire explained the catastrophe as natural phenomena (Mendes-Victor et al., 2008 and Gupta & Gahalaut, 2013). The 1755 earthquake can be considered as the birth of modern seismology, as in 1760 J. Mitchell considered the shakings to be elastic waves propagating in the earth's interior (Vallina, 1999).

However, the quest of the exact earthquake location is still a matter of debate. The 1755 earthquake was not the only tsunamigenic earthquake in the area. The historical reports date back to 60 BC (Mendoça, 1758) and geological evidences were found back to 218 BC by Luque et al. (2001). These authors found three tsunamigenic deposits and suggests an average reoccurrence rate of 2000 years for two consecutive events. His findings also underline that the 1755 event was not the first in this order of magnitude in the area.

In the Portuguese Tsunami catalogue (Baptista & Miranda, 2009) eight events are listed in the 20th century including small and local events. The strongest one was a magnitude 7.9 earthquake on 28th February 1969 in the Horseshoe abyssal plain (Fukao, 1973). The tsunami that followed the earthquake had the maximum amplitude recorded at the tide station of Casablanca with 0.6 m. The tsunami reached the coast in Portugal, approximately thirty minutes (app. 3 a.m. UTC) after the earthquake in low tide conditions. The elevated seismicity and the great earthquake from 1755 raise several questions about the epicentre and the mechanisms acting in the area.

The epicenter location of the earthquakes 1755 and 1969 were somewhere southwest close to the Iberian Peninsula. This area is called Southwest Iberian Margin (SWIM), and it is known for its complex tectonics and heterogeneous morphology. It is composed of various seamounts like the Gorringe Bank, high ridges, low depressions, valleys and an accretionary wedge (see Fig. 1.4). The SWIM is located at the eastern end of the Nubia-Eurasia plate boundary offshore Southwest Iberia and Northwest Morocco. It is as an approximately 1000x400km stretch where the plate boundary is diffuse (Satori et al., 1994; Tortella et al., 1997 and Hayward et al., 1999). The area is characterized by a widespread active seismicity (Cunha et al., 2012).

In consideration of the 1755 earthquake location Johnston (1996) used scale comparison of isoseismal maps of the 28th February 1969 event and suggested the Gorringe Bank, a seamount located about 200 km southwest of Cape St. Vincent as possible candidate source. Baptista et al. (1998b) used hydrodynamic modelling and backward ray tracing to investigate on the source of the 1755 event suggesting a source located closer to the continent. Further investigation revealed several tectonic structures with tsunamigenic potential (Zitellini et al., 1999, García et al., 2003, Terrinha et al., 2003, Gutscher et al., 2002). Some authors suggest to consider multiple rupture scenarios (Zitellini et al., 1999, 2001; Gracía et al., 2003; Ribeiro et al., 2006; Terrinha et al., 2003, 2009) and Matias et al. (2013) suggest for multiple fault rupture events reoccurrence rates of 700 – 3500 yr or less and states that the proximity of the faults should be taken into account.

To better understand the morphology and kinematics of the crust in the SWIM (Sartori et al., 1994, Zitellini et al., 2001, Gutscher et al. 2003, Terrinha et al. 2003, Zitellini et al., 2009) various campaigns have been undertaken using multi-channel reflection seismic, refraction seismic, multibeam swath Bathymetry, and seismic tomography (e.g. ARRIFANO 1992, BIGSETS 1998, SISMAR 2001, SWIM 2009, NEAREST 2010). The analysis and interpretation of this data highlighted several tectonic structures. In the SWIM several considerable NE-SW trending and southeast dipping thrust faults (Zitellini et al., 2009, Matias et al., 2013) could be identified, namely: Gorringe Bank fault, Marques de Pombal fault, São Vincente fault, Horseshoe fault, Tagus Abyssal Plain fault, Coral Patch Ridge, Seine Hills faults, (Hayward et al., 1999; Zitellini et al., 2001; Terrinha et al., 2003; Grácia et al., 2003; Zitellini et al., 2004; Terrinha et al., 2009, Martínez-Loriente et al., 2013) (see Fig. 1.4). Recently Martínez-Loriente et al. (2014) propose the Horseshoe Abyssal plain thrust fault located close to the Horseshoe fault. These thrust faults are intersected by large WNW-ESE trending dextral strike-slip faults called SWIM faults separated in Lineaments North and South (Zitellini et al., 2009). Zitellini et al. (2009) stated the SWIM faults may be in transition from a diffuse to discrete transform plate boundary setting but this theory was later refuted by Cunha et al. (2012). These faults nevertheless prove the recent dextral strike-slip movement (Rosas et al., 2009). In the eastern most part of the Gulf of Cadiz Gutscher et al. (2002) believe to have identified an active subduction dipping eastwards underneath the Gibraltar Arc supported by p-velocity anomalies. The absence of active arc volcanism and instrumental thrust

earthquakes but folding and faulting of young sediments at the Cadiz accretionary wedge and independent movement of the Alboran block causes controversy scientific discussion (e.g. Matias et al., 2013, Duarte et al., 2013). The slab roll back causes extension in the Alboran Sea and is responsible for the westward migration of the Gibraltar Arc. Duarte et al. (2013) states that the Alboran block moves distinctly at velocities of 3-6 mm yr^{-1}, higher than the Africa Eurasia convergence (4 mm yr^{-1}) and additionally induces compressive stresses to the SWIM. Duarte et al. (2013) suggest that both mechanism may lead to passive margin reactivation as the Gibraltar Arc propagates westwards although the migration velocity has been proven to slow down (Gutscher et al., 2012).

However, oblique NW-SE to WNW-ESE striking occurs according to kinematic plate models based on GPS data at rates of 4.5-6 mm yr^{-1} (Sella et al., 2002; McClusky et al., 2003; Fernandes et al., 2003; Nocquet & Calais et al., 2004). Rosas et al. (2012) used analogue and numerical modelling techniques obtaining coherent results and similar morphological features in the corner zone between the strike-slip SWIM faults and the Horseshoe fault. Other recent studies confirm the complexity of the SWIMs interior and state incipient and relic subduction and active thrust faults (Duarte et al., 2013, Monna et al., 2015).

The dynamic processes of the SWIM have been eagerly discussed in literature and two main acting motors have been identified as NW-SE convergence between Africa and Eurasia and westward Gibraltar Arc migration. The importance and future development of each of the contributors is not doubtlessly clarified stressing the need of further investigations. Successive research revealed stepwise more parts of the SWIM puzzle classifying the area as a major source of tsunamigenic earthquakes. Systematized tsunami hazard assessment is required to launch adequate mitigation measures. Especially the tectonic uncertainties confirm the need evacuation measures based on tsunami hazard assessments and an operational tsunami warning system. Further west of the SWIM the Nubia-Eurasia plate boundary is defined as strike-slip fault linked to the Mid-Atlantic Ridge at the Azores triple junction. The eastern segment is called Gloria-Fault a 400km long fault with right lateral slip (Gonzales et al., 1996) and the part at Azores Islands is called the Terceira Ridge. The Terceira Ridge with high moderate seismicity is linked to the Mid-Atlantic Ridge at the Azores Triple Junction (see Fig. 1.3). Common mechanism in the area are normal and transform faulting (Tortella et al. 1997). At the Gloria fault between 24° W and 19° W several large strike-slip events took places in the 20th century (eg. Gutenberg and Richter, 1949; Lynnes and Ruff, 1975 and Grimson and Chen, 1986). The events on 25th November 1941 and 26th May 1975 triggered small tsunamis with maximum amplitudes about 0.45m which were registered in Casablanca (Baptista and Miranda, 2009).

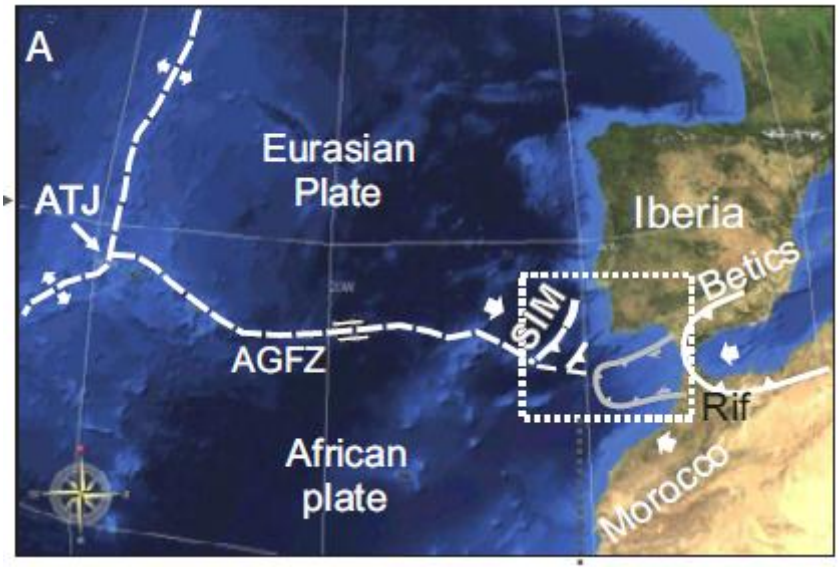

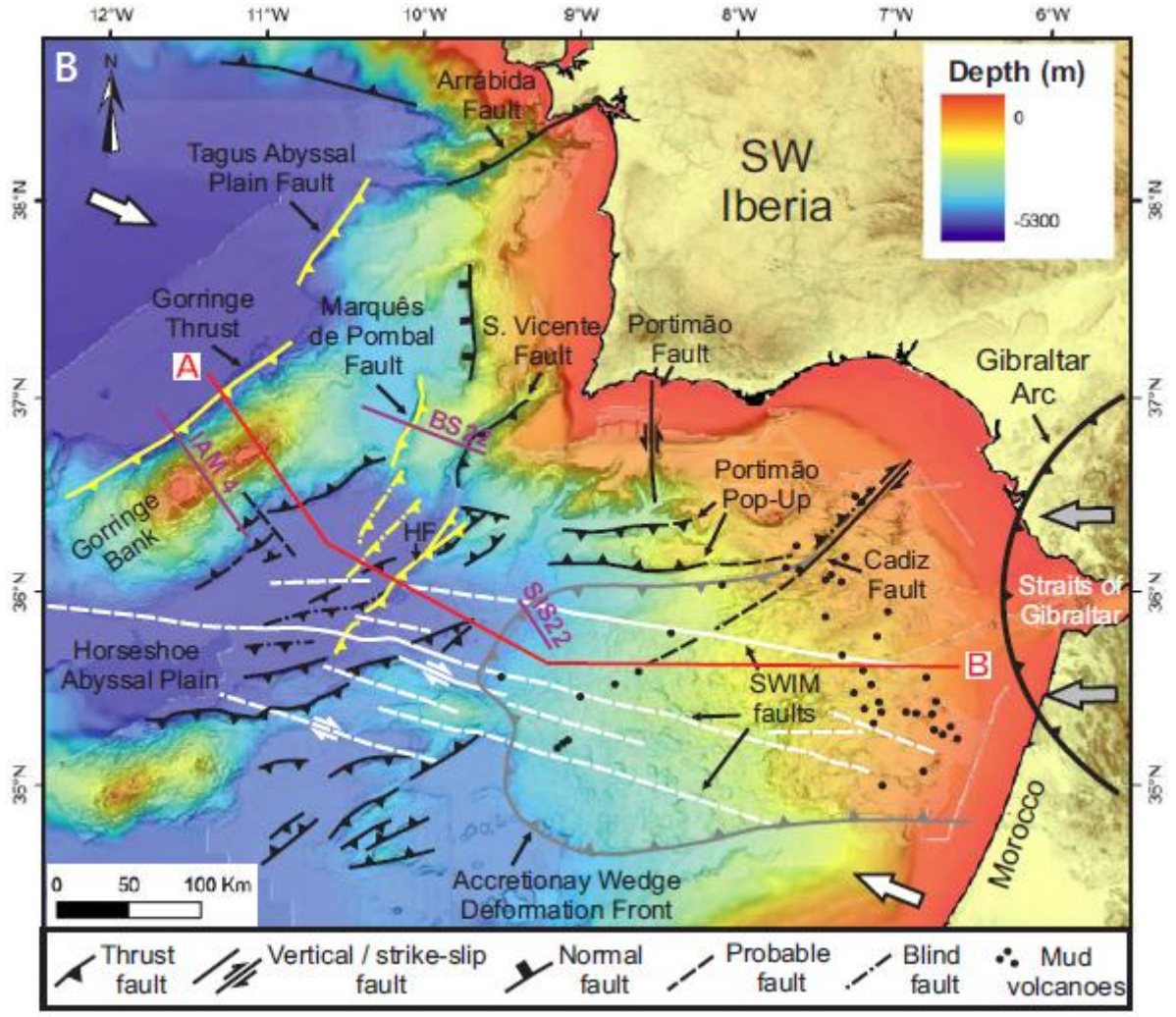

Figure 1.4 A: ATJ – Azores triple junction; AGFZ Azores-Gibraltar fracture zone B: Tectonic map of southwest Iberian Margin (SWIM). Grey arrows show Gibraltar Arc westward movement; white arrows show Africa-Eurasia WNW-ESE convergence. Modified from Duarte et al. (2013)

Concluding, the Portuguese coast is prone to tsunami hazards by local (SWIM) and regional (Gloria fault) source areas. In both areas considerable earthquakes took place and some of them triggered tsunamis. The SWIM is not fully understood and composed of complex tectonic setting. This source area is of specific interest as it triggered the 1755 tsunami and due to the closeness to the Portuguese, Spanish and Moroccan coastlines. Both source areas must be considered when applying the DTHA in study areas located in Portugal, Spain or Morocco.

The earthquake scenarios used to simulate the tsunami impact scenarios in Sines are based on geological evidences. For this thesis the Maximum Credible Earthquake (MCE) and their typical fault (TF) (Miranda et al., 2008; Omira et al., 2009) has been used to produce the tsunami scenarios. This DTHA approach uses the SWIM and the Gloria as seismogenic source areas. Five TFs and their MCE scenarios have been considered to calculate the tsunami scenarios namely: the Gloria Fault (GF), the Cadiz Wedge Fault (CWF), the Gorringe Bank Fault (GBF), the Horseshoe Fault (HSF) and the Marques Pombal Fault (MPF). Additionally a composite rupture model of HSF and MPF (HSMPF) has been built as suggested by (Ribeiro et al., 2006).

2. Methodology

Tsunami hazard assessment is done using two different methodologies: Deterministic Tsunami Hazard Assessment (DTHA) and Probabilistic Tsunami Hazard Assessment (PTHA). This master thesis applies the DTHA approach.

The DTHA method consists of considering certain tsunami events, commonly the most credible earthquake (MCE) scenarios. It provides a description as precise as possible of the effects of large tsunamis that may be triggered by known tectonic and geological processes.

A tsunami hazard scenario corresponds to an event generated by a single or in some cases from multiple sources of fixed dimensions and location, usually corresponding to characteristic earthquakes or to the MCE derived from geological constrains. The chosen scenarios are then modelled numerically and their impact is studied in a specific study area. The methodology is used by a broad scientific community to establish tsunami mitigation measures and for coastal engineering purposes. For that this approach is a valuable tool for coastal disaster management.

2.1. Preparation of the tsunami simulation

For the determination of the single scenarios for DTHA and computation of tsunami propagation and impact for each scenario the benchmarked numerical code NSWING (Non-linear Shallow Water Model with Nested Grids) (Miranda et al., 2014) has been employed.

To model a tsunami numerically several information and data is necessary. The life of a tsunami may be divided in three stages, namely: Generation, Propagation and Inundation, and the same applies to tsunami numerical simulations. The analysis begins in identifying the tsunami source areas and gathering data of the typical faults (TFs) (c.f. paragraph 1.2). These parameters are then used to calculate initial sea surface elevation that constitutes the initial condition to initiate the numerical model. The study area needs to be re-built as a Digital Elevation Model (DEM) describing the bathymetric and topographic features. To better describe the coastal areas high resolution DEMs are needed close to the coast. Depending on the spatial extent from the tsunami source to the study area it is necessary employ a system of coupled nested grids to achieve an adequate resolution in the study area. In this paragraph these stages are described to comprehensively explain the proceeding used in this thesis.

The following steps are carried to launch the NSWING model: (i) *Computation of the initial condition*, (ii) *Preparation of the DEM covering the oceanic path between the source area and the study area*, (iii) *Implementation the DEM in a system of nested grids*, (iv) *Chose the physical quantities to describe the tsunami impact in the study area: run up, flow depth, maximum inundation distance, and launch the simulation.*

(i) *Computation of the initial condition:* First it is necessary to establish the earthquake scenario upon given fault parameters that will generate the tsunami. By knowing the tsunamigenic earthquake source areas and its TFs (Miranda et al., 2008 and Omira et al. 2009) that may affect the study area. It is important to study all possible sources and to use the parameters from the most recent published papers. The initial condition is then computed using the model presented by Okada (1985) embedded in Mirone suite (Luis, 2007). The known fault is drawn upon the parent grid. In this thesis the half minute North Atlantic grid (GEBCO, 2014) has been interpolated to 640m resolution for the parent grid called Layer01. The parent grids extent are from -12.924° W to -5.735° W and from 33.982° N to 39.230 N. This grid embraces all tsunamigenic source areas, the open ocean and the study area. The output of the initial condition is also a finite grid file with the same extensions as the parent grid. After computing the initial conditions for all (TFs) they are stored in a folder, from where the NSWING model is launched later. The theoretical background to model the initial condition is given qualitative manner in paragraph 2.2.

(ii) *Building the DEM:* In a second step the DEM of the study area, the city and port of Sines has been built using GIS tools, namely ArcGIS and QGIS. A number of different data sets containing bathymetric and topographic information have been combined in order to obtain a maximum of detail in the study area. The different data sets used are: a set of high resolution LIDAR data set (Direção-Geral do Território, 2013), a bathymetric model (Instituto Hidrográfico de Portugal,

2012), and a nautical chart (Instituto Hidrográfico de Portugal, 2010). Additionally GPS-RTK (Global Positioning System – Real Time Kinetic) has been applied in areas with missing information. A final resolution of 10 m could be produced and represents the study area properly. Main geological features such as rocky outcrops could be identified in the resulting DEM. A short theoretical introduction on building DEMs for tsunami modelling purposes is presented in paragraph 2.3.

(iii) *Preparations of the nested grids and implementation of the DEM:* To guarantee smooth propagation in the model and numerical stability a system of coupled nested grids has been applied and Courant-Friedrichs-Lewy condition (CFL) must be satisfied. The CFL condition is explained in paragraph 2.4. The resolution of the parent grid is 640m and the resolution of the DEM is 10m. In this step, 2 intermediate girds are produced to reduce the resolution to the scale of 10m in the DEM. A refinement factor of 4 has been applied to achieve the two grids called Layer21 and Layer31 with 160m and 40m respectively. To get smooth propagation of the tsunami when passing from one Layer to the next, the corresponding geographically smaller layers haven been nested using the TINTOL tool embedded in Mirone suite (Luis, 2007). This tool allows to obtain the correct nesting information (correct corner nodes and coordinates) upon the applied refinement factor. This information is than used to produce the higher resolute layer apart from the coarser layer. In the last step the DEM is implemented in Layer31 and nesting information for the Layer41 is produced. This information is than applied on the DEM to get the correct corner nodes and the resulting Layer41. Layer01 to Layer41 are stored together with the initial condition in the folder together with the initial condition. The prepared layers for the nested grids are shown in figure 2.1.

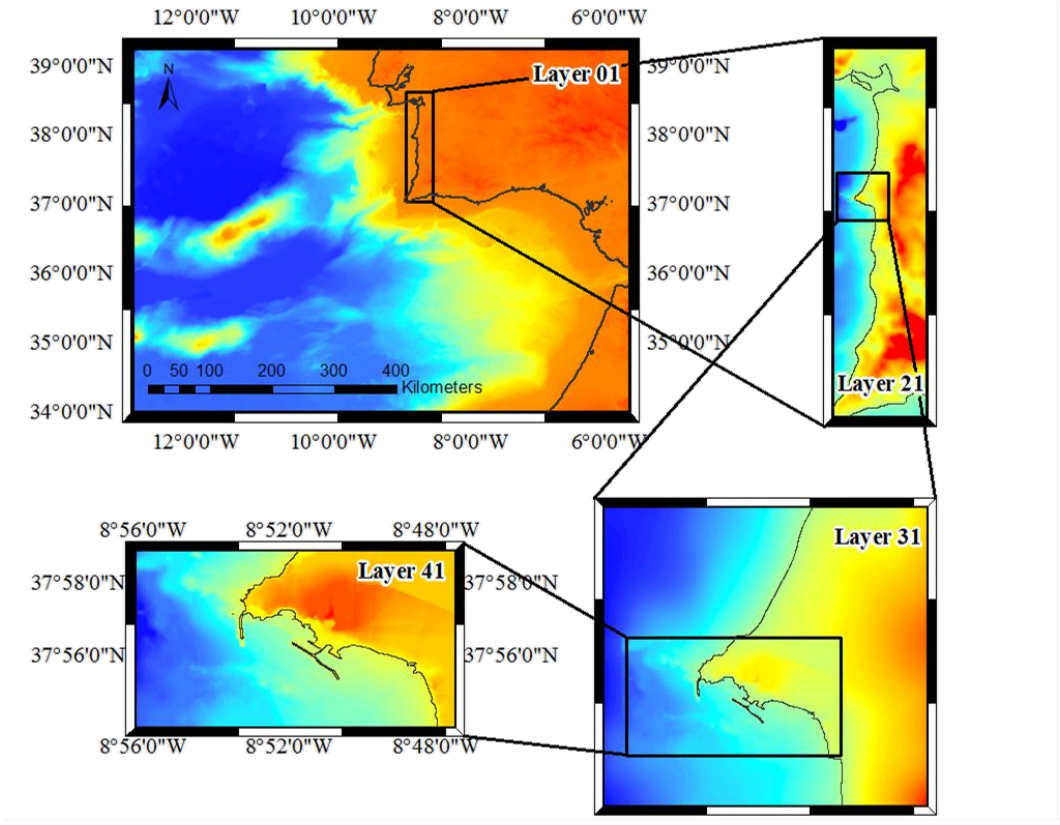

Figure 2.1 Schematic outline of the 4 Layer prepared for NSWING; Layer 41 contains the DEM.

(iv) *Definition and launching the tsunami simulation:* The NSWING operational files and the files described from (i) to (iii) are sufficient if prepared correctly to launch a tsunami simulation. To do this an executable batch file must be edited, so that NSWING can use the prior prepared files. Additionally to the files to be used operators are extended to calculate the information wanted. In

this study we additionally prepared a list in format DAT with geographical coordinates corresponding to the positions of the virtual tide gauges. NSWING reads this file and stores the free surface elevation in this point for a chosen time step. This way waveforms can be analysed and compared with existing records. The computation tsunami propagation and inundation are described in paragraph 2.4 and 2.5 respectively.

With the DTHA approach physical quantities such as wave height, flow depth, drawback, inundation extent or velocities can be approximated. These quantities serve to draw scenario maps, develop vulnerability studies and evacuation measurements. Maximum current speed is also an important parameter that can be mapped if the vulnerability of buildings or coastal structures is in focus of the study. Tsunami travel time maps show the first arrivals of the waves in the study area. Virtual tide gauges can be placed to analyse the waveforms arriving at the test site. Information such as polarity, period, maximum wave height at the tide gauges and attenuation time can be obtained. As the tide regime in the Atlantic is strong, i. e. there is a significant difference (of the order of meters) between high tide and low tide, the scenarios must include this effect. An aggregate scenario can be produced plotting the MWH and the MFD in each cell considering the contribution of the individual scenarios (Tinti et al., 2011).

The final results are presented in integrated hazard maps for all the considered and the aggregate scenario. The integrated hazard maps have been produced using GIS tools. Each integrated hazard map consists of MWH, MFD, MRU and MDB of the corresponding scenario. The static effect of tides is analysed for three different tidal stages mean lower low water (MLLW), mean sea level (MSL), and mean higher high water (MHHW). Further the contribution of each scenario to the aggregate tsunami impact at MSL condition has been calculated. The analysis of the waveforms produced at chosen virtual tide gauges provide information such as, arrival time, period, the biggest wave and attenuation time.

2.2. Generation of tsunamis in the source area

Tsunami are triggered by submarine earthquakes, landslides, volcanic eruptions or meteorite impacts. As stated earlier this thesis focuses on studying the tsunami hazard caused by earthquakes. They occur at or near to tectonic faults for example along plate boundaries. Three types of faults can be distinguished: strike-slip or transform faults, normal faults and thrust or invers faults. The movement along pure strike-slip faults is horizontally and usually do not cause tsunamis. In some cases rupture mechanism along these faults may also have a vertical component and have the potential to trigger a tsunami. Normal and inverse faults cause vertical seabed motion and they are capable to lift or lower the water column above triggering the motion at the sea surface. Inverse faults may have contributions of horizontal components.

The initial sea surface deformation is computed using the analytical formulae, after Mansinha & Smylie (1971) synthetized in Okada (1985). They represent the displacement field on the surface of an elastic half-space, when a dislocation of given direction and size is introduced at a given epicentral depth. The deformation is then transferred to the free surface assuming that the water layer above is considered as incompressible layer and the seabed deformation is transferred directly to the free surface of the ocean (Kajiura, 1970).

To compute the seabed deformation one needs information on the earthquake mechanism: fault plane parameters, magnitude and distribution of deformation along the fault plane.

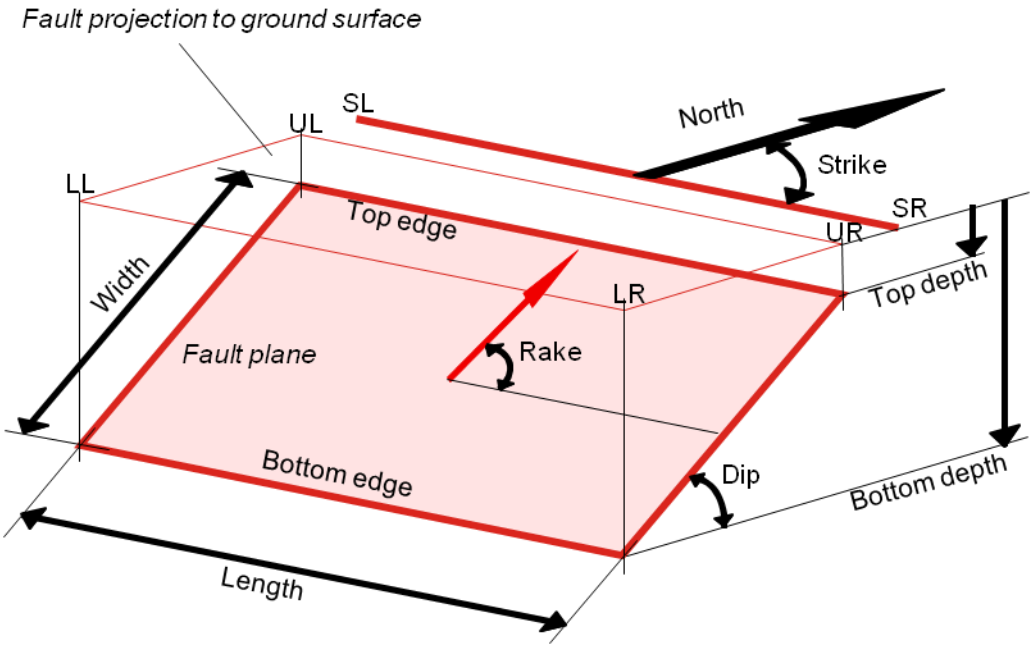

Figure 2.2 Definition of an individual seismogenic source. (Istituto Nazionale di Geofisica e Vulcanologia, 2015)

The fault plane parameters are the length, L, the width, W, the slip – dislocation along the fault plane and the angles, strike, dip, rake & depth. Length and Width give the extensions of the fault plane. Strike, dip and rake are given in angular units. The strike is the angle relative to the north on a horizontal plane and describes the trending of the fault. The dip measures the inclination from the planar horizontal surface. And the rake gives the direction of the movement along the fault plane during a rupture in relation to the strike. The distances of the movement along the rake is given by the slip and is measured in meters. In figure 2.2 the described fault parameters are represented. Upon these variables the initial tsunami condition is calculated employing Okadas (1985) model and set to the sea surface to initiate propagation.

These model has some limitations as the rupture area is simplified to a rectangle and the rupture process is considered to instantaneous. Dutykh (2008) and Dutykh & Dias (2007) showed that this model is not appropriate tsunami earthquakes with slower rupture mechanism. However, in this study the application of the model is justified as it has been used for medium sized thrust faults and an instantaneous rupture can be assumed (Omira, 2010).

The seismic moment (Aki, 1972) is related to shear modulus μ, the rupture area A and the slip D

$$M_0 = \mu A D \tag{2.1}$$

Where μ is the shear modulus in (Pa), A is the rupture area (m²) and D is the mean net displacement on A in (m).

However, important to state is that the seismic moment depends on the three factors. But only two of them may have direct influence on tsunami generation. The slip is the movement that describes the dislocation along the fault plane. Greater slip values produce greater amplitudes. And greater areas of the fault plane produce higher periods. The shear modulus μ, thus is a property of the crust in the region and has no impact on the tsunami but on the resulting seismic moment M_0 and the moment magnitude, M_w.

The moment magnitude serves to quantify the earthquakes strength. It was derived by Kanamori (1977) and is linked with the scalar seismic moment, M_0. This scale has the big advantage that it does not saturate as other magnitude scales, for earthquakes stronger than magnitude 8.

$$M_w = \frac{2}{3}\log_{10}(M_0) - 10.73 \quad (2.2)$$

Table 3.1 in paragraph 3 summarizes all used fault parameters to calculate the initial conditions for the in paragraph 1.2 presented tsunami scenarios. The initial conditions for all considered tsunami scenarios have been computed in Mirone suite (Luis, 2007) that employs Okadas (1985) model.

2.3. Digital Elevation Model

In order to represent in sufficient quality the study area digital data of bathymetric and topographic features and/or charts are combined. The DEM is built in a Geographic Information System and the final output is a simple grid dataset where each cell has a single numerical elevation value. The resolution of the resulting DEM defines quality of the entire numerical tsunami model Tinti et al. (2011).

Tsunami propagation close to the coast and on land is critically dependent on the small scale effects; so, the DEM (digital elevation model) must be able to represent the most significant coastal features and the shoreline accurately. The DEM, representing the bare earth, was produced including: (i) the tsunami source area and the test site areas along the coast (ii) good horizontal resolution in the test areas in order to assure a full description of local effects (iii) continuity offshore-onshore in particular in respect to the vertical datum.

The information used to build the DEM may be vector or raster/grid data containing height or depth information. Vectorised datasets can be point, line or polygon information corresponding to different altitudes such as bathymetric or topographic contours of various charts or individual point measurements like individual gathered GPS data. On the other hand raster data contains equal sized squares as cells, where each cell represents its corresponding height information. Each dataset is given in a horizontal and vertical spatial reference system which is usually depending on the geographical location, spatial extent, and producing institution or end-user. For instance bathymetric charts for nautical purposes are commonly referenced to bathymetric zero and topographic data is usually set in relation to MSL. One must be aware to while DEM preparation to set all used data sets in the same reference system. These datasets are available in different qualities. A raster dataset with smaller cell size contains more detailed information as a dataset with bigger cell size. When combining two or more different datasets it is necessary to give preference to more accurate data to avoid ambiguities. The vectorised datasets may improve the final DEM especially if the available raster data is of poor quality. It is crucial to transform all used data in the same horizontal and spatial reference system. In a final step the resulting DEM should be evaluated and verified for instance by posterior GPS-measurements at specific control points. A 3-D representation also helps to avoid errors for example at dataset boundaries. The resulting DEM is presented in Fig. 2.3.

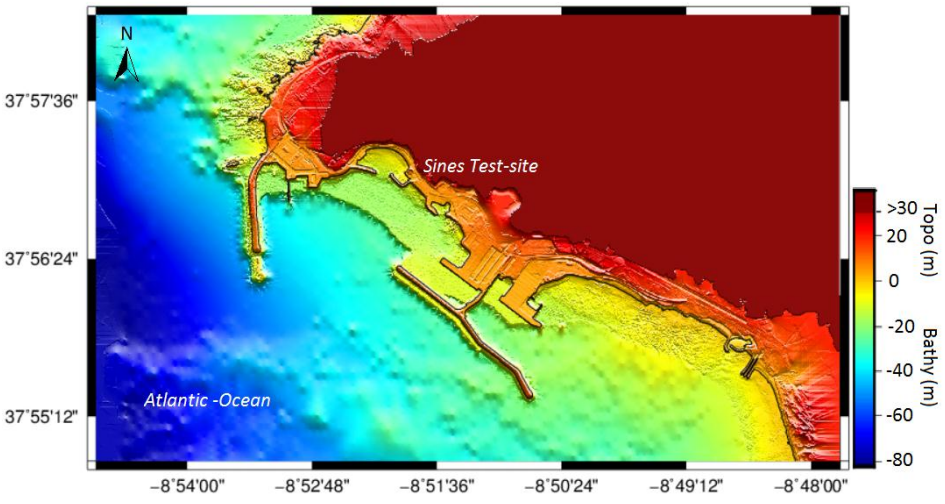

Figure 2.3 Resulting digital elevation model (DEM) of Sines test-site.

2.4. Tsunami Propagation & SWEs

The motion of any viscous fluid substances and gas is described by the Navier-Stokes Equations, which are based on the Newton's second law conservation of momentum in three dimensions. In combination with the conservation of mass a system of four coupled nonlinear partial differential equations are formed for three velocity components and pressure. There is no complete analytical solution for these coupled system of equations. Approximations are introduced to obtain best possible solutions depending on the scale of the geophysical process to be studied. This thesis applies the shallow water model which neglects viscous forces and the depth integrated SWEs average vertical velocities and accelerations. Other models to simulate tsunamis are the Boussinesq long wave model and the complete fluid dynamic model. The SWEs remain the most used model used by computational codes. In the last two decades numerical codes like TUNAMI-N2 (Imamura 1995), MOST (Titov and Synolakis 1995; 1998), COMCOT (Liu et al., 1998) and more recently UNIBO-TSUFD (Tonini et al., 2011 & Tinti et al., 2013) have been developed to model with sufficient accuracy tsunami propagation and coastal impact. To start propagation all these codes apply the model presented by (Okada 1985) described in paragraph 2.2. However, all these models are based on the SWEs but use different numerical methods to solve them. This study uses the recently developed and benchmarked code NSWING (Non-linear Shallow Water Model with Nested Grids) (Miranda et al., 2014). NSWING has been benchmarked following the definitions presented by Synolakis (2006). It is entirely written in C and applies core parallelisation enhancing computational performance.

The equations that govern the motion of tsunamis are called Navier-Stokes Equations. They represent Newton's conservation of momentum in three dimensions in a cartesian frame (x,y,z) (2.3a, 2.3b and 2.3c). These three equations in combination with the equation of conservation of mass (2.3d) build a system of four coupled non-linear partial differential equations.

$$x: \rho\left(\frac{du}{dt} + f_* w - fv\right) = -\frac{\partial p}{\partial x} + \frac{\partial \tau^{xx}}{\partial x} + \frac{\partial \tau^{xy}}{\partial y} + \frac{\partial \tau^{xz}}{\partial z} \tag{2.3a}$$

$$y: \rho\left(\frac{dv}{dt} + fu\right) = -\frac{\partial p}{\partial y} + \frac{\partial \tau^{xy}}{\partial x} + \frac{\partial \tau^{yy}}{\partial y} + \frac{\partial \tau^{yz}}{\partial z} \tag{2.3b}$$

$$z: \rho\left(\frac{dw}{dt} - f_* u\right) = -\frac{\partial p}{\partial z} - \rho g + \frac{\partial \tau^{xz}}{\partial x} + \frac{\partial \tau^{yz}}{\partial y} + \frac{\partial \tau^{zz}}{\partial z} \tag{2.3c}$$

$$\frac{\partial \rho}{\partial t} + \frac{\partial}{\partial x}(\rho u) + \frac{\partial}{\partial y}(\rho v) + \frac{\partial}{\partial z}(\rho w) = 0 \tag{2.3d}$$

where x-, y- and z- axes are the coordinates in directions eastward, northward and upward respectively. The variables, u, v and w represent the velocity components in x, y and z directions, $f = 2\Omega \sin\varphi$ is the Coriolis parameter and φ is the latitude, $f_* = 2\Omega \cos\varphi$ is the reciprocal Coriolis parameter (which is neglected for the most geophysical approximations), where Ω is the rotation rate of the earth, ρ is the density, p is the pressure, g is the gravitational acceleration and the τ terms represent normal and shear stresses because of friction.

To solve these equations appropriate approximations are used depending on the scale of the geophysical motion to be studied. The considered approximations are applied to the Navier-Stokes equations to reduce them to the SWEs. To obtain the SWEs viscous stresses and any flow gradients in vertical direction are eliminated (Synolakis, 2006) which is considered as a valid approximation for long waves if $h \leq \frac{\lambda}{25}$ (Intergovernmental Oceanographic Commission, 2013) is satisfied. The water body is assumed to be incompressible. The SWEs are derived by a depth average integration from the ocean bottom to the free surface and it is assumed that pressure distribution is hydrostatic everywhere. This allows to introduce the variable η the free surface elevation through the hydrostatic approximation for the pressure, $p = \rho g(d + \eta)$, where d is the water depth. This assumption is valid and considered to deliver results with sufficient accuracy as tsunamis are considered as long waves propagating in shallow water as stated in the paragraph 1.2. The shallow water model calculates the evolution of the water surface and the depth averaged water particle velocity.

The SWEs may be used in their linear or non-linear form. The linear SWEs consists in neglecting the non-linear terms: non-linear convective inertia forces and the bottom friction terms. They are considered valid for open ocean propagation if the wave amplitude is much smaller than the ocean depth. The linear version of the SWEs without Coriolis Effect is represented in equations (2.4a-c).

$$\frac{\partial \eta}{\partial t} + \frac{\partial P}{\partial x} + \frac{\partial Q}{\partial y} = 0 \tag{2.4a}$$

$$\frac{\partial P}{\partial t} + gD\frac{\partial \eta}{\partial x} = 0 \tag{2.4b}$$

$$\frac{\partial Q}{\partial t} + gD\frac{\partial \eta}{\partial y} = 0 \tag{2.4c}$$

where η is the free-surface displacement, $D = d + \eta$ is the total water depth, and d is the still-water depth. P and Q represent the horizontal components of the volume flux along the x- and y- coordinates respectively.

The non-linear SWEs include the non-linear convective inertia forces and bottom friction which become increasingly important when tsunami travels into shallower water. NSWING solves linear and non-linear SWEs. For the DTHA approach in this study non-linear solutions have been calculated for all instances of the time. The non-linear SWEs are given in Equations (2.5a-c)

$$\frac{\partial \eta}{\partial t} + \frac{\partial P}{\partial x} + \frac{\partial Q}{\partial y} = 0 \tag{2.5a}$$

$$\frac{\partial P}{\partial t} + \frac{\partial}{\partial x}\left(\frac{P^2}{D}\right) + \frac{\partial}{\partial y}\left(\frac{PQ}{D}\right) + gD\frac{\partial \eta}{\partial x} + \tau_x = 0 \tag{2.5b}$$

$$\frac{\partial Q}{\partial t} + \frac{\partial}{\partial x}\left(\frac{PQ}{D}\right) + \frac{\partial}{\partial y}\left(\frac{Q^2}{D}\right) + gD\frac{\partial \eta}{\partial y} + \tau_y = 0 \tag{2.5c}$$

where η is the free-surface displacement, $D = d + \eta$ is the total water depth, and d is the still-water depth. P and Q represent the horizontal components of the volume flux along the x- and y- coordinates respectively, τ_x and τ_y are the bottom friction terms in x- and y- directions, respectively.

In spherical coordinates including Coriolis parameter the coupled system of equations yields

$$\frac{\partial \eta}{\partial t} + \frac{1}{R\cos\varphi}\left[\frac{\partial P}{\partial \psi} + \frac{\partial}{\partial \varphi}(\cos\varphi Q)\right] = -\frac{\partial d}{\partial t} \tag{2.6a}$$

$$\frac{\partial P}{\partial t} + \frac{1}{R\cos\varphi}\frac{\partial}{\partial \psi}\left(\frac{P^2}{D}\right) + \frac{1}{R}\frac{\partial}{\partial \varphi}\left(\frac{PQ}{D}\right) + \frac{gD}{R\cos\varphi}\frac{\partial \eta}{\partial \psi} - fQ + \tau_x = 0 \tag{2.6b}$$

$$\frac{\partial Q}{\partial t} + \frac{1}{R\cos\varphi}\frac{\partial}{\partial \psi}\left(\frac{PQ}{D}\right) + \frac{1}{R}\frac{\partial}{\partial \varphi}\left(\frac{Q^2}{D}\right) + \frac{gD}{R}\frac{\partial \eta}{\partial \varphi} + fP + \tau_y = 0 \tag{2.6c}$$

where η is the free-surface displacement, $D = d + \eta$ is the total water depth, and d is the still-water depth. P and Q represent the horizontal components of the volume flux, φ and ψ represent the latitude and longitude of the Earth respectively, f is the Coriolis parameter $f = 2\Omega\sin\varphi$ and φ is the latitude, where τ_x and τ_y are the bottom friction terms in x- and y- directions, respectively.

The bottom friction terms are evaluated by the Manning formula (c.f. equations 2.7a-b).

$$\tau_x = \frac{g\, n^2}{H^{\frac{7}{3}}} P \sqrt{P^2 + Q^2} \tag{2.7a}$$

$$\tau_x = \frac{g\, n^2}{H^{\frac{7}{3}}} P \sqrt{P^2 + Q^2} \tag{2.7b}$$

where n is the Manning's roughness coefficient.

The Manning's formula is an empirical model approximation to simulate different roughness conditions that applies different roughness coefficients depending on the bottom conditions. Linsley and Franzini (1979) for instance presented different values for the Manning's roughness coefficient for varying conditions in a channel. When considering the worst case tsunami scenario Manning's roughness coefficient is set to zero (Omira 2010).

For the numerical solution the presented SWEs need to be discretised. The discretization process implements replacing the derivatives in the SWEs by finite difference approximations. To do this the numerical code models the problem in a grid with finite cells (c.f. paragraph *(iii)* in 2.1). The differential equations are discretised in the grid model scheme to formulate an algebraic system of equations. This system of equations follows a specific scheme to compute the solutions for the SWEs in each cell of the grid model at specific time steps. For each cell (i,j) in each instant of time the discretised set of algebraic equations are solved upon the conditions of the prior time step. The initial condition launches the propagation at time step, $t = 0$. NSWING adopts an explicit staggered finite leapfrog numerical scheme for linear terms (Liu et al. 1998) and an upwind scheme for non-linear terms. The choice of the time step must satisfy the CFL (Courant-Friedrichs-Lewy) condition to ensure numerical stability. The linear CFL condition is shown in equation (2.8) and NSWING uses 0.5 as C_{max} value.

$$C = u * \frac{\Delta t}{\Delta x} \leq C_{max} \tag{2.8}$$

2.5. Tsunami inundation & Run up

To model the inundation on dry land a moving boundary scheme is used. The overland inundation is a complicated task as at includes interaction with the impacting wave with the shore line. In order to obtain reliable results for nearshore propagation and on land inundation a high resolution DEM is crucial. To calculate inundation a specific numerical algorithm is employed to propagate the incident wave on dry land. This algorithm must be updated each time step and for each grid cell to simulate the moving shoreline appropriately. This moving boundary algorithm compares if the total water depth is high enough to inundate neighbouring dry grid cells, along each of the two directions. In case of neighbouring grid cell inundation the algorithm must be update with the new shoreline for the next time step.

The study area is modelled in the DEM as finite gird containing dry cells "land" and wet cells "water" which are separated by the shoreline. A simplified one dimensional stepwise model is presented in figure 2.4 to visualize the inundation proceeding.

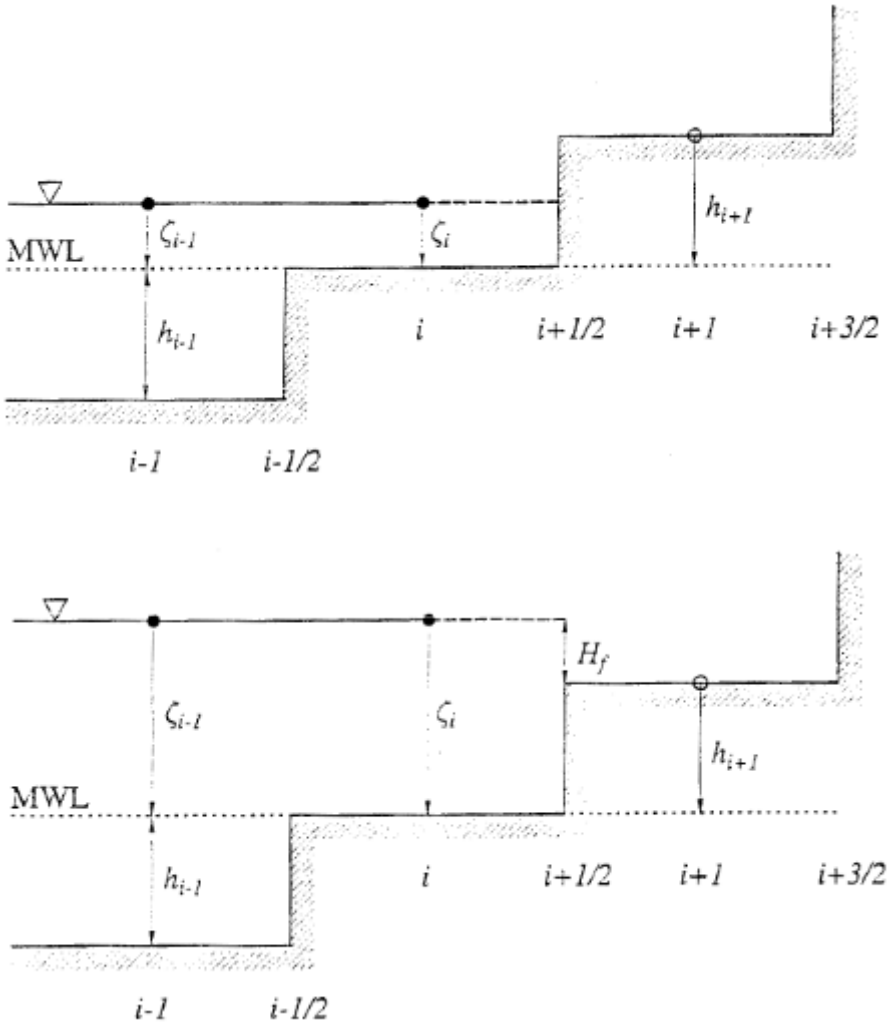

Figure 2.4 Illustration of the inundation algorithm in one dimension as presented in Liu et al. (1998) and Wang (2009) for 2 cases and MWL is the Mean Water Level.

The one dimensional inundation is presented for two cases which can be considered as different time steps in the simulation (Fig. 2.4). Using this procedure the following algorithm that computes the flood depth at each time step is derived (Liu et al., 1998):

(i) In case $H_{i+1} \leq 0$ and $h_{i+1} + \eta_i \leq 0$, then the shoreline stays between grid cells i and $i + 1$ and the volume flux $P_{i+1/2}$ remains 0.

(ii) In case $H_{i+1} \leq 0$ and $h_{i+1} + \eta_i \geq 0$ the shoreline moves to between grid cells $i + 1$ and $i + 2$ and the volume flux $P_{i+1/2}$ might be nonzero. But the volume flux $P_{i+3/2}$ is defined to be zero. The resulting inundation depth is given by $H_f = h_{i+1} + \eta_i$.

(iii) In case $H_{i+1} \geq 0$, the shoreline is dislocated to between grid cells $i + 1$ and $i + 2$. The volume flux $P_{i+1/2}$ might be nonzero and the volume flux $P_{i+3/2}$ has to be zero. The inundation depth is given by $H_f = \max(h_{i+1} + \eta_i; h_{i+1} + \eta_{i+1})$.

3. Application

In this paragraph the application of the described methodology is presented. The outcome of the study has been submitted to the scientific journal Natural Hazards and Earth System Sciences in June 2015 and is under discussion. The paper can be accessed at http://www.nat-hazards-earth-syst-sci-discuss.net/3/4663/2015/nhessd-3-4663-2015.pdf. The DTHA approach has been used to study the tsunami impact from multiple local and regional sources on the test site in Sines, Portugal. The results show heavy inundations in the port and surrounding areas.

Scenario based approach for multiple source Tsunami Hazard assessment for Sines, Portugal

M. Wronna[1],* , R. Omira[1,3] , M. A. Baptista[1,2,3]

1 Instituto Português do Mar e da Atmosfera, IPMA, I. P., Lisbon, Portugal

2 Instituto Superior de Engenharia de Lisboa, Lisbon, Portugal

3 Instituto Dom Luiz, University of Lisbon , IDL, Lisbon, Portugal

* Correspondence to: M. Wronna, IPMA, Rua C do Aeroporto, Lisbon, Portugal

(martinwronna@gmail.com)

Abstract

In this paper, we present a scenario-based approach for tsunami hazard assessment for the city and harbour of Sines - Portugal one the test-sites of project ASTARTE. Sines holds one of the most important deep-water ports which contains oil-bearing, petrochemical, liquid bulk, coal and container terminals. The port and its industrial infrastructures are facing the ocean southwest towards the main seismogenic sources. This work considers two different seismic zones: the Southwest Iberian Margin and the Gloria Fault. Within these two regions, we selected a total of six scenarios to assess the tsunami impact at the test site. The tsunami simulations are computed using NSWING a Non-linear Shallow Water Model With Nested Grids. In this study, the static effect of tides is analysed for three different tidal stages MLLW (mean lower low water), MSL (mean sea level) and MHHW (mean higher high water). For each scenario, inundation is described by maximum values of wave height, flow depth, drawdown, run-up and inundation distance. Synthetic waveforms are computed at virtual tide gauges at specific locations outside and inside the harbour. The final results describe the impact at Sines test site considering the single scenarios at mean sea level, the aggregate scenario and the influence of the tide on the aggregate scenario. The results confirm the composite of Horseshoe and Marques Pombal fault as the worst case scenario. It governs the aggregate scenario with about 60% and inundates an area of 3.5km².

Keywords: Tsunami hazard assessment, numerical modelling, aggregate scenarios

1 Introduction

Tsunamis are low frequency but high impact hazards for coastal societies. The December 26th, 2004 Indian Ocean and the March 11th, 2011 Tohoku striking tsunami events raised awareness due to the enormous loss of life and property. The Indian Ocean event in 2004 demonstrated the need for operational early warning systems around the world. However, seven years later, the 2011 Tohoku event showed the limitations of the scientific knowledge concerning tsunami sources, coastal impacts, and mitigation measures. Since then, in the NEAM region (North East Atlantic, Mediterranean and connected seas) many efforts have been addressed to understand better the tsunamigenic sources and to improve the tsunami hazard assessment capabilities. Within the NEAM region, the Gulf of Cadiz is among the most tsunami hazardous areas. The historical reports include events dated back to 60 BC

(Mendonça, 1758, Baptista and Miranda, 2009; Kaabouben et al., 2009), but the geological evidence show high energy events back to 7000 years BP (Luque et al., 2001).

The Portuguese coast is highly exposed to tsunami threat from local and regional active tectonic sources. The main tsunamigenic area is the SWIM (South West Iberia Margin), with a number of considerable SE dipping inverse faults (Zitellini et al., 2009, Matias et al., 2013). The most severe tsunami was the 1st November, 1755 caused by the Lisbon earthquake with an estimated magnitude of 8.5 by Martins and Mendes Victor (1990). This magnitude was more recently re-evaluated by Solares and Arroyo (2004) with an estimate of 8.5±0.3. The tsunami hit the entire northern Atlantic basin with huge impact in Iberia and Morocco (Baptista and Miranda, 2009). In the 20th century, the 28th February 1969 earthquake with a magnitude of 7.9 (Fukao, 1973) caused a small tsunami of 0.5 m amplitude in Lagos and Cascais (Baptista et al., 1992; Baptista and Miranda, 2009). The tsunami waves hit the coast circa 3 a.m. in low tide conditions (Baptista et al., 1992) but no significant damage was observed.

The second tsunamigenic zone to be considered is the Gloria Fault. The Gloria fault is a segment of the Eurasia-Nubia plate boundary. It is a large strike slip fault, located between 24ºW and 19ºW, with scarce seismic activity but was nonetheless the location of several large events during the 20th Century, in particular the 25th November 1941 earthquake, a submarine strike-slip event of magnitude 8.3-8.4 (Gutenberg and Richter, 1949) and the 26th May 1975 with magnitude 7.9 (Lynnes and Ruff, 1975; Grimson and Chen, 1986).

In recent years, a considerable number of tsunami hazard assessment studies were published for the North East Atlantic area. Most of these studies focus on the tsunami impact in the Gulf of Cadiz using a scenario based approach namely: Lima et al. (2010), Omira et al. (2010), Omira et al. (2011), Atillah et al. (2011), Baptista et al. (2011a), Renou et al. (2011), Omira et al. (2013), Benchekroun et al. (2013) and Lemos et al. (2014). Recently, Omira et al. (2014) published a probabilistic tsunami hazard assessment for the North East Atlantic.

In this study, we use a Deterministic Tsunami Hazard Assessment (DTHA) approach to evaluate the tsunami impact in Sines. The study area contains the country's most important deep water port which is connected to big industrial complexes by fragile infrastructure such as pipelines and conveyor belts. In summer the city is a popular tourist destination.

The DTHA approach consists of studying the impact of specific tsunami events – tsunami scenarios - in the study area. The impact is described in terms of maximum wave height (MWH), maximum flow depth (MFD), maximum run up (MRU) and maximum drawback (MDB). We further built the aggregate scenario plotting the MWH in each cell considering the contribution of the individual scenarios (Tinti et al., 2011).

The final results are presented in integrated hazard maps for all the considered and the aggregate scenario. Each integrated hazard map consists of MWH, MFD, MRU and MDB of the corresponding scenario. The static effect of tides is analysed for three different tidal stages mean lower low water (MLLW), mean sea level (MSL), and mean higher high water (MHHW). Further we present the contribution of each scenario to the aggregate tsunami impact at MSL condition.

2 Study area and Digital elevation model

Sines is a city located on the west littoral margin of the Iberian Peninsula about 150km south of Lisbon (Fig. 3.1 a). The study area includes the city of Sines and parts of the surrounding municipality covering a coastline of about 35 km. The city has approximately 15000 inhabitants (Instituto Nacional de Estatística, 2011) and about 5000 floating population because of economic and touristic purpose.

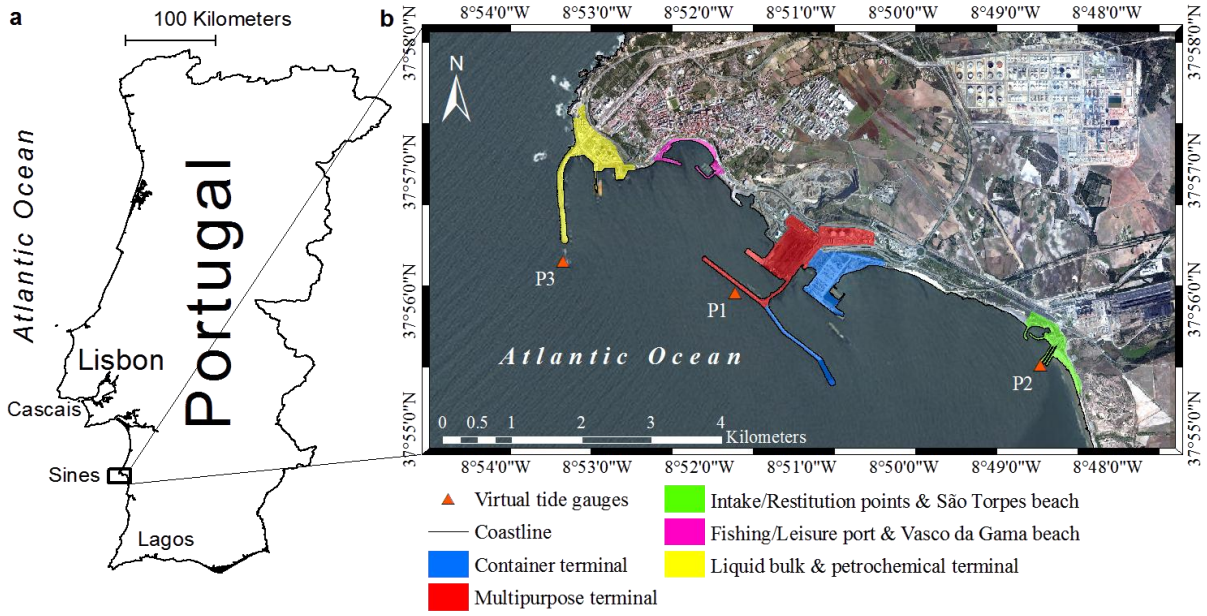

Figure 3.1 (a) General map: Location of Sines test site; (b) test site map identifying general features and tide gauges for synthetic wave forms.

Sines plays a major role in terms of energy production and storage. There are 2 great production centres of oil and gas industry (GALP refinery and Repsol YPF petrochemical industrial complex) which are connected via pipelines to oil-bearing and petrochemical terminal of Sines harbour (Câmara Municipal de Sines, 2007). The harbour is the country's most important deep water port (with 28 m depth) situated south of the city centre and consists of 5 terminals: liquid bulks, liquid natural gas, petrochemical, container and multipurpose; as well as fishing and leisure ports (Porto de Sines, 2014). The liquid natural gas terminal (LNG) contains facilities for loading and unloading processes of methane carriers, expedition facilities at LNG terminal depot, three LNG storage tanks, LNG processing facilities and natural gas dispatch facilities for the pipeline connecting the Sines LNG terminal to the Natural Gas Transport Network. At the multipurpose terminal coal is stored in stockpiles and is transported by a conveyor belt to Sines thermoelectric power plant. The power plant uses seawater for cooling of the generators which is captured and returned at the intake and restitution points close to São Torpes beach (Fig. 3.1 b). The majority of the harbour facilities and big areas of the power plant are situated in possible inundation area below the 25m topographic contour. The liquefied natural gas storage deposits is located right behind the port. In case of a destructive tsunami, facilities or leaking pipelines raise the danger of explosion and may cause an environmental disaster.

The study area limits are East to West from 8°47'00" to 8°55'00" and North to South from 37°58'00" to 37°55'00". In the northern part the landscape is designed by the influence of the magmatic batholith of Sines with a steep and rocky seafront. On the south westernmost part of the rocky outcrops begins the area of the port. The main jetty is facing south with a maximum elevation of 15m above MSL and a width of 10m (figure 3.1 b). The Liquid Bulks Terminal and Petrochemical Terminal are protected by the jetty against strong swell reaching the Portuguese coast mainly from northwest. The smaller jetties protect the fishing and leisure ports, which also protect the shell-shaped beach "Vasco da Gama" (see figure 3.1 b). Northwards is located the city centre and the majority of domestic property on the top of the batholith with altitudes higher than 25m above sea level. Further east, the remaining terminals: multipurpose, container and natural gas protected by a recently enhanced jetty of approximately 2.5km length (see figure 3.1 b). The container terminal is currently under construction due to expansion at the easternmost area of the port exposing new economic value to tsunami threat. Further southeast at the coast are situated the jetties to protect the intake and restitution points of the EDP thermoelectric power plant. Right beyond the jetties southwards begins the popular highly visited beach of "São Torpes" which is already a part of the natural park "Costa Vicentina" (see figure 3.1 b). The main port areas and Vasco da Gama beach have their coastline facing southwards. The main tsunamigenic sources are

located south of the study area. Due to its openness and exposure to the sea, the impact of tsunamis and other marine hazards like sea level rise are of great concern for the area.

In order to guarantee a good representation of the study area, we built a high-resolution Digital Elevation Model (DEM). We combined three different datasets and set them to the same reference system using GIS tools (Geographic Information System). We validated the final dataset using real time kinetic GPS on field trips. The DEM is crucial for computation of inundation on the dry land and near shore propagation.

Different types of datasets were used: a set of high resolution LIDAR dataset (Direção-Geral do Território, 2013), a bathymetric model (Instituto Hidrográfico de Portugal, 2012), and a nautical chart (Instituto Hidrográfico de Portugal, 2010). The LIDAR data-set of 2011 has a resolution of 2m. The data is available in PT-TM06/ETRS89 projection and referenced to hydrographic zero 2m underneath MSL. The data-set of the bathymetric model contains a grid based point information 100m spacing based on hydrographic surveys. In the overlapping areas of LIDAR data-set and the bathymetric model preference has been given to the more recent and higher resolution LIDAR data-set. For further improvement, the nautical chart of Sines (The nautical chart of Sines consists of 2 different charts one showing a more detailed view of the port with a scale of 1:12500 and the general chart of the test-site with a scale of 1:30000) was scanned, geo-referenced, and digitized. Depth and altimetry data of the bathymetric model and the nautical charts are referenced to the hydrographic zero. All data was referenced to MSL which lays 2m above hydrographic zero in Sines. In order to validate the final datasets we used data field surveyed data points with GPS-RTK (Global Position System Real Time Kinetic). In order to fill gaps of the LIDAR data we used GPS RTK collect data to implement a recently constructed extension of a jetty not yet present in the data-sets. After combination, validation and adaption of the existing data-sets a grid representing the final study area with 10m resolution has been computed. The resulting DEM properly represents Sines test-site, especially the near shore areas, as LIDAR-Data set is of very high resolution. The 10m grid represents small rocky outcrops of the batholith in between Vasco da Gama beach and the leisure port. Other features like the connection to the main jetty in front of the Multiuse, Liquid Natural Gas- and Container-terminal or the jetty at the leisure port suffer from the low resolution.

3 Numerical Model and Nested Grids

Numerical modelling of tsunamis is commonly divided into three stages: generation, propagation, and inundation. We use an in-house developed and benchmarked numerical code NSWING (Non-linear Shallow Water Model with Nested Grids) (Miranda et al., 2014) to model the tsunami. The model supposes an instant seabed deformation that has been rendered using the half-space elastic theory (Okada, 1985) embedded in Mirone suite (Luis, 2007). The vertical sea bottom deformation is assumed to be equal to the free surface deformation and transferred to the ocean surface.

The code solves linear and non-linear approximations of shallow water equations (SWEs) to calculate tsunami propagation and inundation in a Cartesian or spherical reference system. In the deep ocean nonlinear convective inertia forces are of secondary order as waves travel with amplitudes much smaller than water depths. When the tsunami enters shallow coastal areas, the non-linear convective inertia force and bottom friction become increasingly important. We applied non-linear SWEs approximations in all instances, for deep-ocean, near-shore and on-shore propagation.

NSWING employs a dynamically coupled system of nested grids and solves SWEs using an explicit staggered finite leapfrog numerical scheme for linear terms and an upwind scheme for nonlinear terms. The code further applies a radiating boundary condition, allowing wave motion pass from one domain to other, through boundaries with very small reflections. A moving boundary algorithm (Liu et al., 1995), based on “wet” and “dry” cells, is adopted to track shoreline movement while inundation.

Propagation and behaviour of tsunamis change because of varying bathymetry when entering coastal areas. To model the impact in Sines we implement a dynamically coupled system of nested grids. We interpolated the half minute North Atlantic grid (GEBCO, 2014) to 640m resolution for the parent grid. Using four layers and applying a refinement factor of 4 we achieved 10m final resolution in the DEM.

The amplitude of the tide in south-west Portugal is above 2m and must be taken into account in Sines. (Baptista et al., 2011a) To study the tide effect, the tidal variation of the last three years have been considered. We used the values of Mean High Water (MHW) and Mean Low Water (MLW) from 2012 to 2014 and calculated the mean to obtain the MHHW and MLLW respectively and referenced them to MSL. The MHHW is 1.22m above the MSL and the MLLW 0.88m underneath the MSL. These values have been subtracted and added respectively to the established DEM. For each designed scenario we ran the model in MHHW, MSL and MLLW conditions to study the static influence of the tide and is presented in the aggregate scenario (Antunes, 2014).

4 Tsunamigenic Scenarios

To design the tsunami scenarios we use the main seismogenic source zones and the associated Maximum Credible Earthquake (MCE) (Miranda et al., 2008 and Omira et al., 2009). We used the typical fault (TF) for each MCE. In this study we use the TF presented in Omira et al. (2009).

The seismogenic sources used here are SWIM and Gloria. For this study we considered four TFs in the SWIM area and their MCE scenarios to reproduce initial condition for tsunami propagation namely: the Cadiz Wedge Fault (CWF), the Gorringe Bank Fault (GBF), the Horseshoe Fault (HSF) and the Marques Pombal Fault (MPF) (Fig. 3.2). Additionally we use a seismogenic scenario consisting of a composite rupture of HSF and MPF (HSMPF), believed to have caused the 1st November 1755 event (Ribeiro et al., 2006).

The major tsunami event in the SWIM is the one associated with the 1st November 1755 earthquake and the exact source remains unknown. Numerous studies and campaigns have been carried out in order to solve the quest of the 1st November 1755 tsunamis source. Data (multi-channel reflection seismic, refraction seismic, multi beam swath Bathymetry) has been gathered to reveal more accurate information of the tectonic in the SWIM. These investigation in the SWIM revealed numerous geological evidences of the used TFs. Several authors proposed distinct sources for this event.

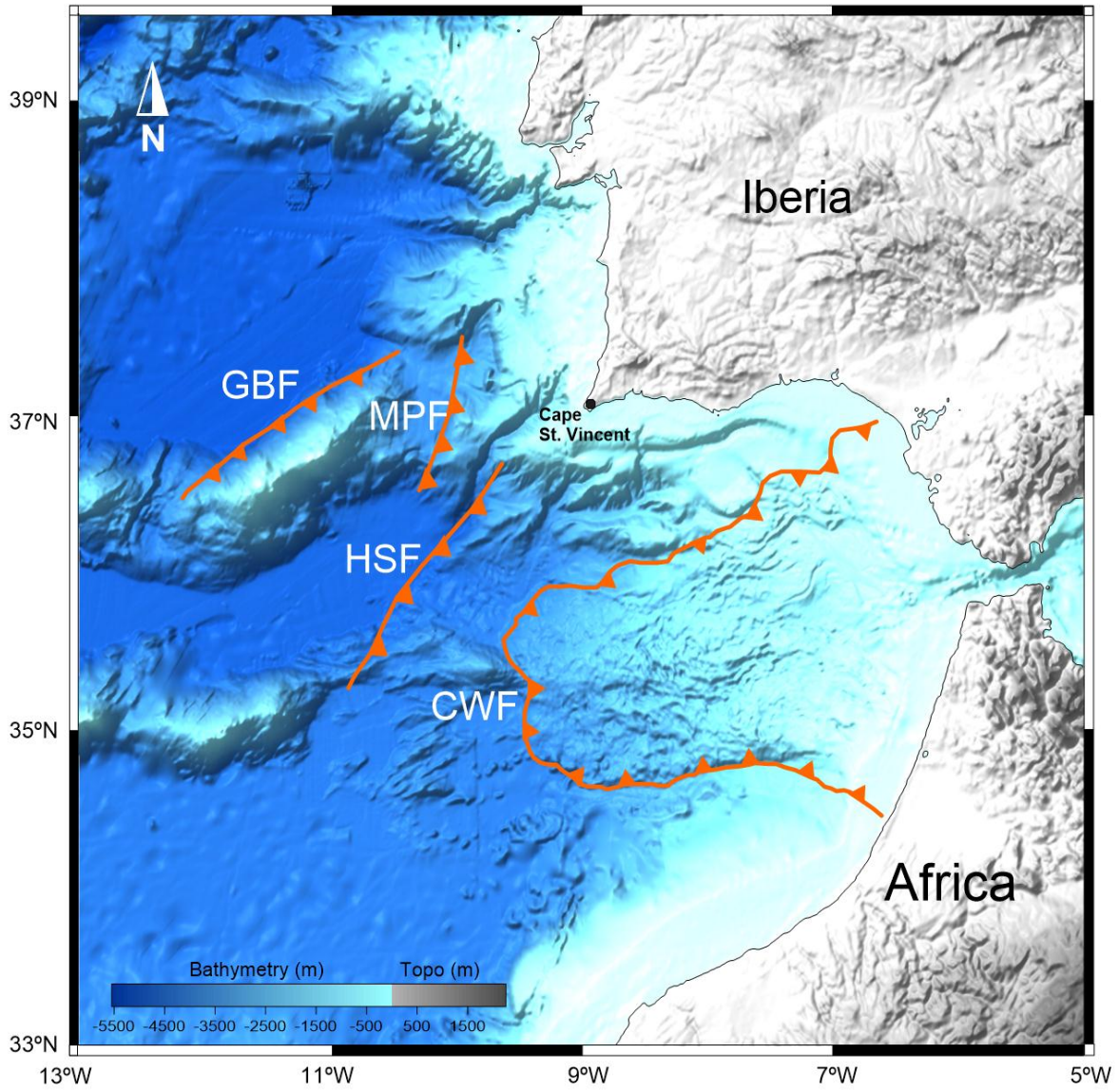

Figure 3.2 TFs used for Tsunami modeling in the SWIM. Dextral reverse faults: Gorringe Bank fault (GBF), Marques Pombal fault (MPF), Horseshoe fault (HSF); Subduction slab: Cadiz Wedge Fault (CWF).

Johnston (1996) suggested the GBF as a possible candidate source of the 1st November 1755 event through scale comparison of isoseismal maps with the 28th February 1969 event (c.f. Fig 3.2). Using tsunami backward ray tracing methods Baptista et al., (1998) suggested a source location for the 1755 Tsunami closer to the Portuguese coast. Zitellini et al. (1999) found an active thrust fault, the MPF through interpretation of multi-channel seismic data (c.f. Fig 3.2). Gutscher et al. (2002) concluded that the identified active subduction, the CWF is a candidate source for 1755 event and must be considered in natural hazard assessments (c.f. Fig 3.2). Further neo-tectonic structures and deformed seafloor sediments at the HSF also show clusters with shallow seismicity (Gràcia et al., 2003) (c.f. Fig 3.2). Some authors suggest to consider multiple fault rupture scenarios to explain the high magnitude observed in 1755 (Zitellini et al., 2001, Gràcia et al., 2003, Ribeiro et al., 2006, Mendes-Victor et al., 2005). Nevertheless the exact source of the 1755 Lisbon event is still a matter of discussion. These uncertainties related to 1755 source and the tectonic processes acting in the SWIM confirm the need of systematic tsunami hazard assessment in surrounding areas.

The Gloria zone is our far field source area. The Gloria fault is a transform fault running from 24° West to 19° West (Laughton and Whitmarsh, 1974). Three strong magnitude earthquakes occurred in the last 130 years: 22 December 1884 (Moreira, 1984), 25 November 1941 – Magnitude 8.3 (Gutenberg and

Richter, 1949, Moreira, 1984) and 25 May 1975 – magnitude 7.9 (Lynnes and Ruff, 1975 and Grimson and Chen, 1986). The 25 November 1941 and the 26 May 1975 produced small tsunamis recorded in the tide stations in the North East Atlantic basin (Debrach, 1946, Moreira, 1984, Baptista et al., 1992, Baptista and Miranda, 2009). The 25 November 1941 epicenter location and the focal mechanism are presented in Baptista et al. (2011b). We used these parameters to draw a 1941 like scenario for the Gloria source zone. The TF parameters are presented in table 3.1 and the fault is presented in figure 3.3.

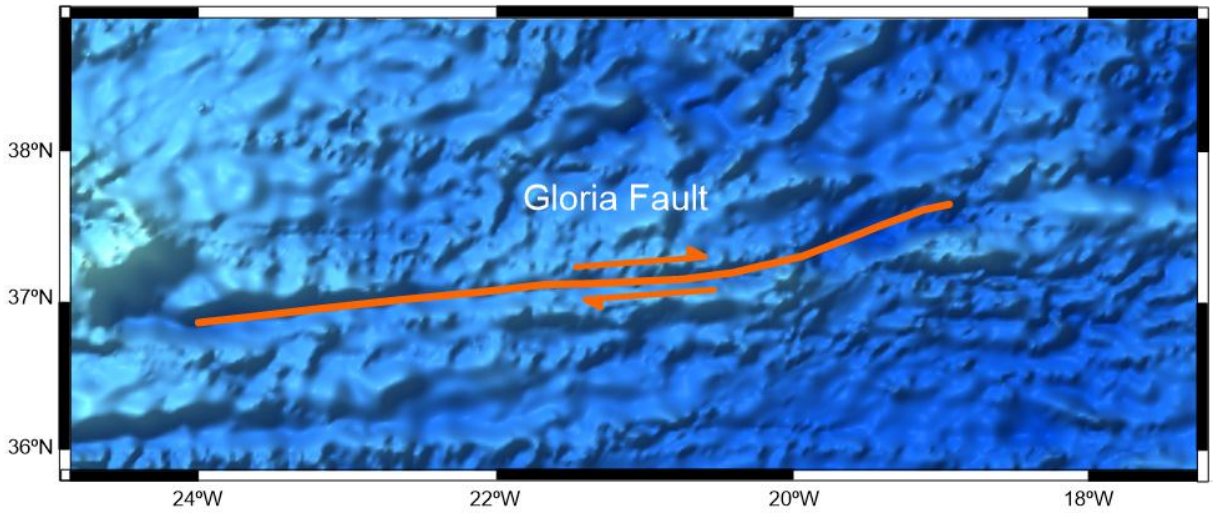

Figure 3.3 Dimension and geographic location of the Gloria fault (red line) considered in this study.

Table 3.1 Fault parameters of the tsunamigenic sources considered in this study.

Fault	L [km]	W[km]	Rake [°]	Strike [°]	Dip [°]	Slip [m]	Depth [km]	μ [Pa]	Mw
HSF	165	70	90	42.1	35	15	5	4.5e+10	8.5
MPF	110	70	90	20.1	35	8	5	4.5e+10	8.25
CWF	170	200	90	349	5	20	5	3.0e+10	8.75
GBF	200	80	90	53	35	10	5	4.5e+10	8.5
HSMPF	165/ 110	70/ 70	90/ 90	42.1/ 20.1	35/ 35	15/ 8	5/ 5	4.5e+10/ 4.5e+10	8.75
Gloria	200	50	160	82	88	11	1	3.0e+10	8.3

5 Results

We ran a total of eighteen simulations. For each typical fault we considered three tide conditions: Mean Lower Low Water (MLLW), Mean Sea Level (MSL) and Mean Higher High Water (MHHW). The results are presented in integrated maps of maximum wave height (MWH), maximum flow depth (MFD), maximum drawback (MDB) and maximum run up (MRU) (Fig. 3.4 a-e). For the scenarios at MSL, we additionally present synthetic waveforms (Fig. 3.5 and 3.6) at chosen positions (Fig. 3.1-b).

In figure 3.7 we present the aggregate scenario considering all calculated models. Figure 3.8 shows the inundation and the drawback limits considering the aggregate scenarios at the three tide conditions.

5.1 MSL Results

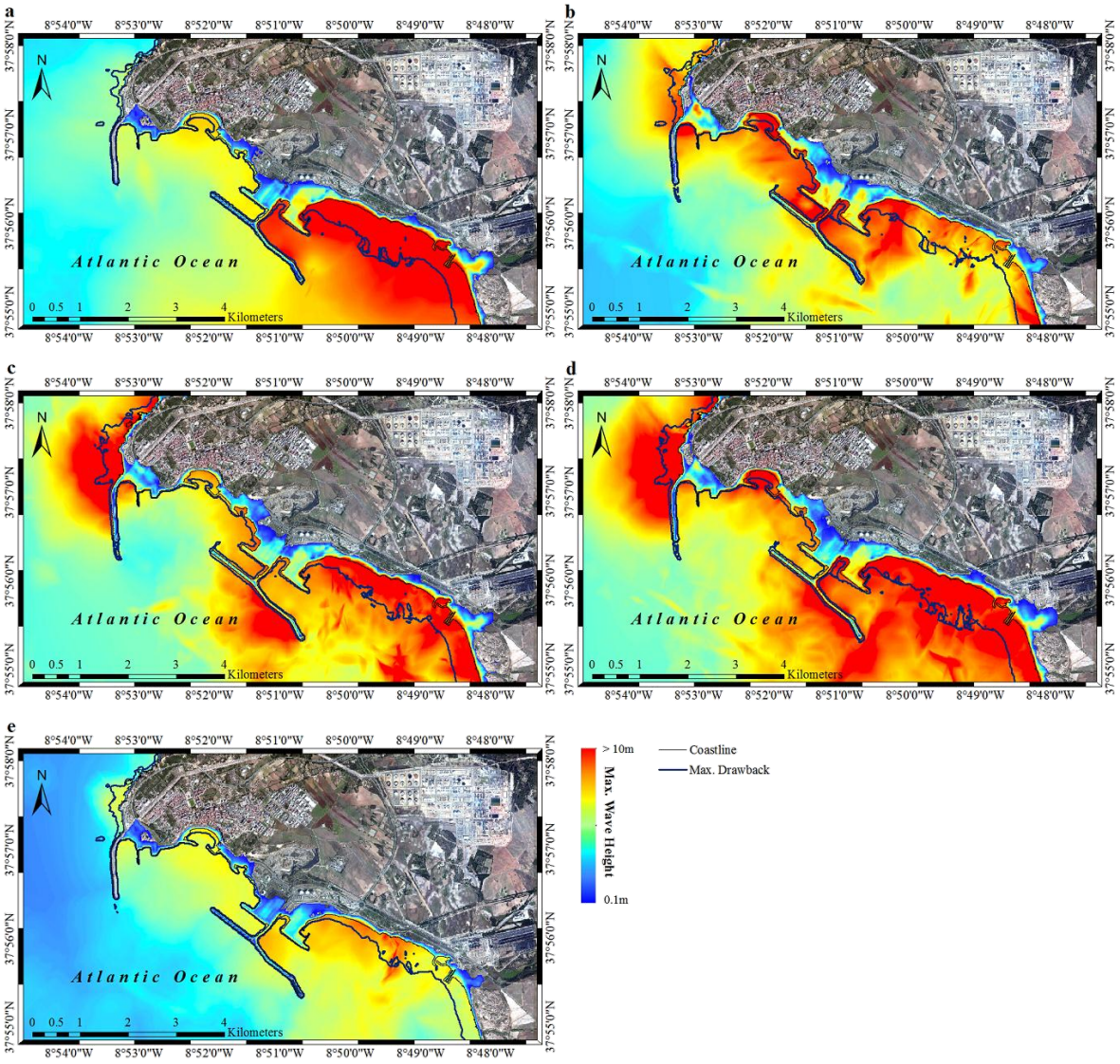

Figure 3.4 Results of MWH, MFD, MDB and MRU of the SWIM scenarios considering MSL: (a) CWF, (b) GBF, (c) HSF, (d) HSMPF, (e) MPF.

The analysis of figures 3.4 and 3.5 shows that all SWIM scenarios produce heavier inundation and drawback in comparison to the Gloria fault scenario. The Gloria scenario produces MWH values of approximately 1m while the SWIM scenarios produce MWH above 10m. Figures 3.4-3.6 present results of the individual scenarios and their absolute values are summarized in table 3.2. The HSMPF scenario,

corresponding to the worst case scenario, produces 18.6m of MWH and 3.47 km² of inundated area. Detailed analysis of figure 3.4-d shows flow depths greater than 0.5m in 90% of the inundation area.

The GBF and HSF scenarios, with MWH above 15m, also produce inundation above 3 km² (cf. table 3.2 and Fig. 3.4-b and Fig. 3.4-c). The remaining SWIM scenarios (CWF and MPF) still produce MWH above 10m and leave more than 2 km² inundated.

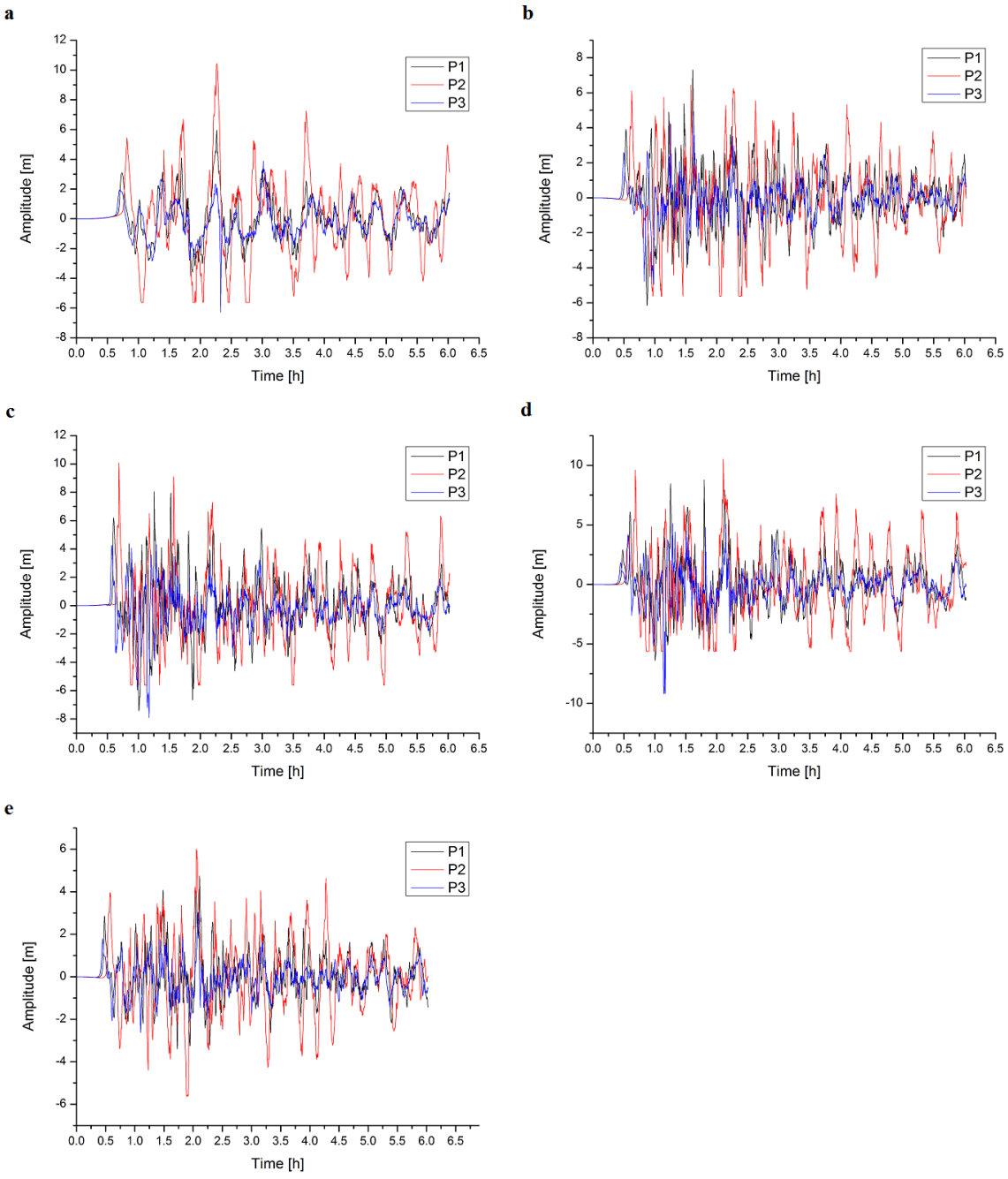

Figure 3.5 Synthetic waveforms for 6h propagation time at 3 chosen points (cf. Fig. 3.1) for the SWIM scenarios: (a) CWF, (b) GBF, (c) HSF, (d) HSMPF, (e) MPF.

Among the SWIM scenarios, the MPF produces the weakest impact in Sines but still with MWH above 10m (cf. Fig. 3.4-e). MRU, up to 19.3m occurs during the HSF scenario at the south of the test site. All SWIM scenarios produce sufficient drawback (see blue lines in Fig. 3.4 a-e) to leave the intake and restitution points of the thermoelectric power plant dry. MDB occurs during the composite tsunami

model HSMPF. The Gloria scenario produces 1.2m MWH in certain areas and inundates low lying areas such as beaches. The flooded area of the Gloria scenario is less than 0.2km² and the area at the intake and restitution points does not stay dry (Fig. 3.6-a and Table 3.2).

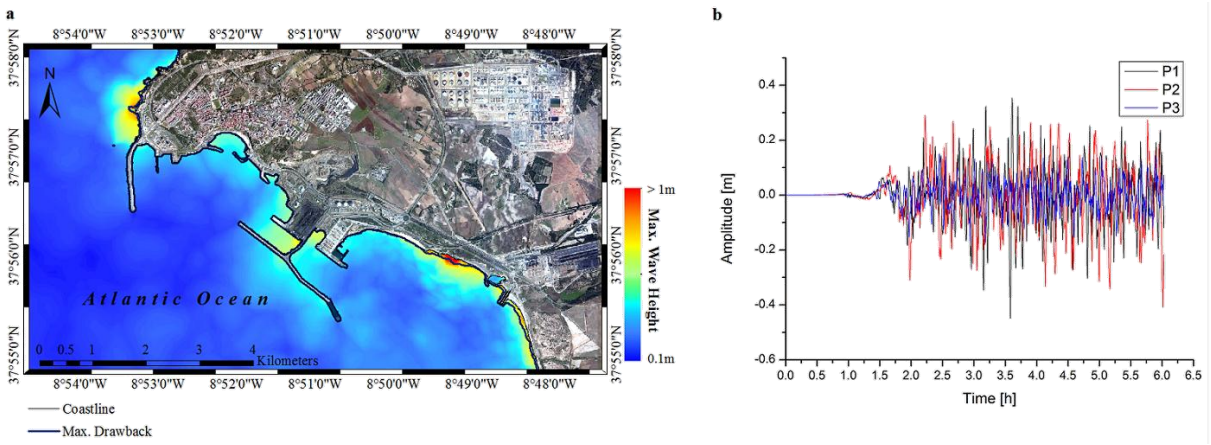

Figure 3.6 (a) Results MWH, MFD, MDB and MRU for the Gloria scenario, (b) synthetic waveform for 6h propagation time a 3 chosen points (cf. Fig. 3.1) for the Gloria scenario.

The analysis of the synthetic waveforms at the virtual stations shows similar periods and tsunami travel time (see figure 3.5) for all SWIM scenarios. First arrival occurs in all records at point P3 (blue curves in Fig. 3.5 and Fig. 3.6-b). Clearly distinguishable are the records for the Gloria scenario presented in Fig. 3.6-b which shows an arrival time of about 85 minutes after initial sea surface displacement. The maximum amplitude is about 0.4m with a period of approximately 10 minutes (Fig. 3.6-b). The record in tide gauge point P2, at 5.6m depth right in front of the intake and restitution points, confirms that no considerable drawback is happening throughout the event (Fig. 3.6-b). The records of the SWIM scenarios GBF, HSF, HSMPF, MPF show periods of 15 to 20 minutes and for the CWF approximately 25 minutes. Maximum amplitudes are obtained at the tide gauge P2 for the tsunamis produced by CWF at the 3rd wave, HSF and HSMPF at the 1st and 3rd wave, respectively. At point P2 waveforms indicate that the cell stays at least once dry for all SWIM scenarios (Fig. 3.5). Attenuation is visible for all scenarios after 6 hours runtime except for the Gloria scenario where attenuation occurs after 15 hours.

Table 3.2 Synthesis of the Results: MFD, MWH, inundated area, MDB, MRU and arrival time for all scenarios at MSL.

Scenario (MSL)	MFD [m]	MWH [m]	Inundated Area [km²]	MDB [km²]	MRU [m]	Arrival Time [min]
CWF	12.2	12.8	2.71	2.98	14.1	38
HSF	13.3	15.7	3.16	3.37	19.3	30
GBF	12.4	17.1	3.18	3.02	18.9	25
HSMPF	13.1	18.6	3.47	3.80	17.5	22
MPF	9.1	10.7	2.07	1.98	11.3	22
Gloria	0.9	1.2	0.19	0.22	4.3	85

5.2 The aggregate scenario and the influence of the tide

The aggregate scenario map depicts the extreme hazard values field point by takin the envelope of all individual scenarios. We present aggregate scenarios of MWH, MFD, MDB and MRU for the different tide conditions (Fig. 3.7).

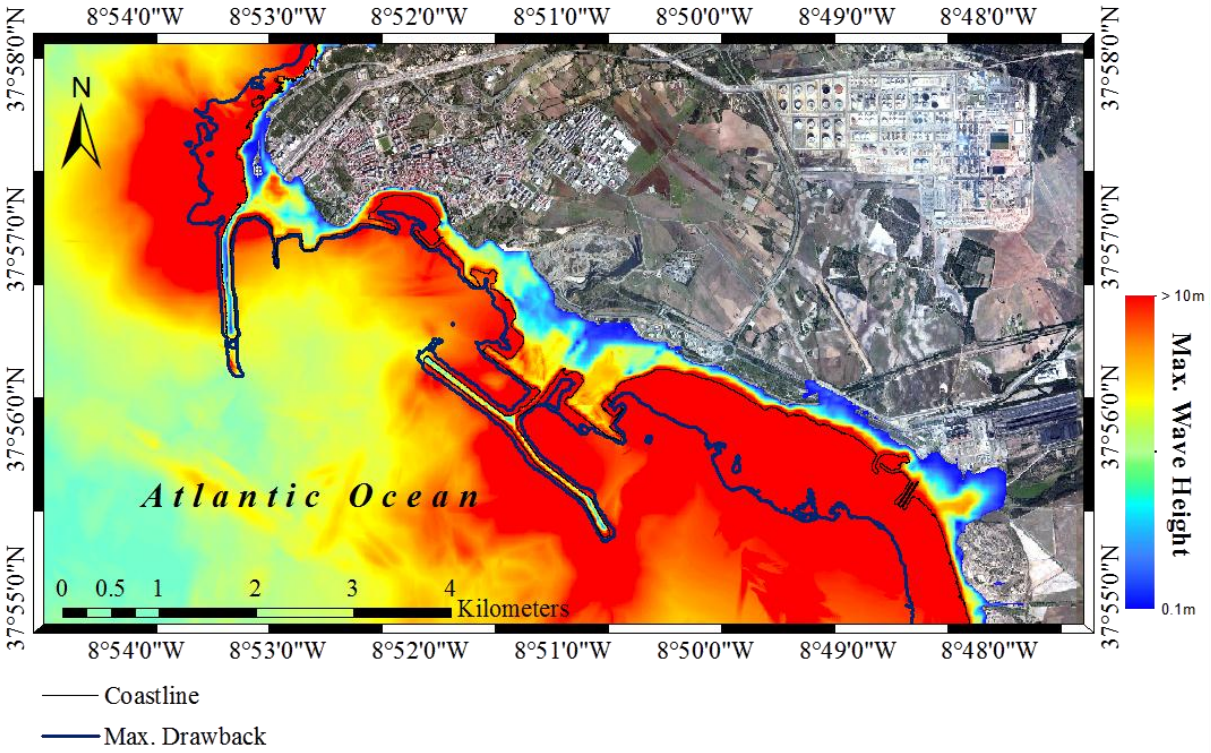

Figure 3.7 MWH, MFD, MDB and MRU for the aggregate scenario considering all stages of the tide.

The aggregate scenario map (Fig. 3.7), considering all stages of the tide, shows 4.8km² MDB area and 4.1km² maximum inundated area. MRU values over 20m occur close to the cliffs at Vasco da Gama beach and is reached in MHHW condition. In other areas, such as behind the liquid bulks and petrochemical terminal and at the railway connection to the port, MRU values exceed 15m. MWHs above 10m have been modelled along the entire coastline (Fig. 3.7). In high tide condition the inundation area is over 4km² and 3.5km² in low tide condition considering the aggregate scenario. Inundation area is 5% bigger at MSL and 14% at MHHW compared to MLLW (Fig. 3.8). MDB area is 16% greater at MLLW and 11% greater at MSL than in MHHW conditions (Fig. 3.8). The flooded area at Vasco da Gama beach is not significantly bigger at MHHW as the area behind the beach is confined by the steep topography. Moreover figure 3.7 shows that the mean MFD values are about 1.5m higher at MHHW than at MLLW in the area of the beach. Other areas behind the multipurpose and container terminal or at São Torpes beach show clearly greater inundation areas in high tide condition (Fig. 3.8). The limits of MDB and MRU for the aggregate scenario concerning MLLW, MSL and MHHW are mapped in figure 3.8.

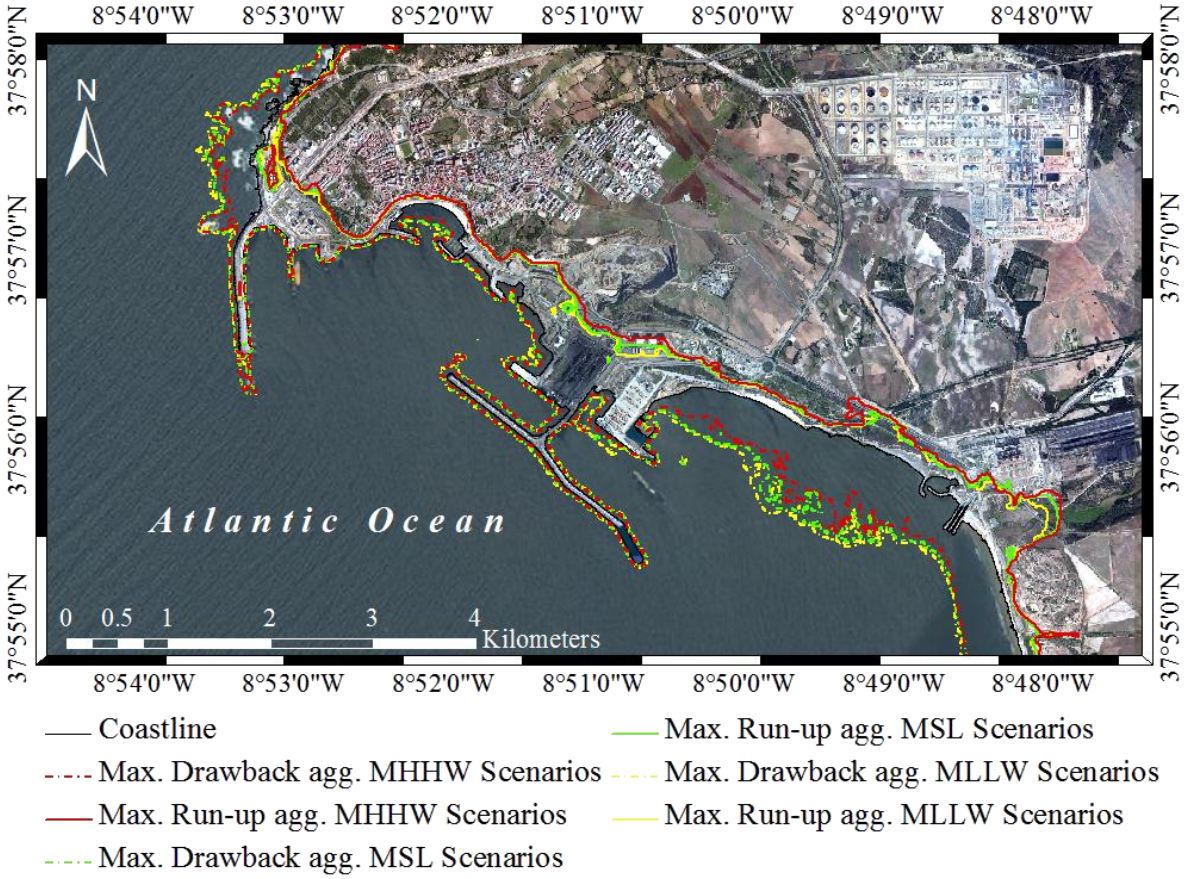

Figure 3.8 MDB and MRU limits for the stages MLLW, MSL and MHHW of the tide.

6 Discussion and Conclusions

We ran a total of 18 scenarios to study the tsunami impact at Sines. Our results show that all SWIM scenarios cause severe inundation and drawback. To complement the integrated hazard maps of MWH, MFD, MDB and MRU we recorded synthetic waveforms at chosen points (see figure 3.1). The signals of the waveforms are diverse. This fact may be explained due to differences in the TF parameters. Waveforms from HSF, MPF, GBF and HSMPF are comparable in terms of period and arrival time (Fig. 3.5a-e). These TFs are dextral reverse with SW-NE trending and the hanging block in the SE. They are all located in the SWIM area. They are distinguishable through their dimensions and slip. Other parameters like strike, dip and rake are similar. Among the single fault scenarios the GBF is the biggest single fault producing 17.1m MWH in the study area (see table 3.2). The HSF, although smaller, produces a similar inundation and wave height pattern as the slip is 5m higher compared to the GBF (see table 3.1). The MPF is smaller in terms of dimensions and has a slip of 8m and therefore produces the weakest tsunami in the SWIM (Table 3.1 and Fig. 3.4-e). Nevertheless, MWHs are above 10m and MPF is the nearest fault to the test-site, that produces short tsunami travel time (22 minutes in figure 3.5-e). The composite scenario HSMPF is the worst case scenario and combines the effects of both faults: First wave arrives 22 min after the earthquake and tsunami triggered by HSMPF causes worst inundation and drawback in Sines. The CWF is a subduction slab and has different fault parameters compared to the other TFs in the SWIM. The shallow east dipping slab has dimensions of 170x200km and a slip of 20m (see table 3.1). The analysis of the waveforms shows that wave periods generated by the CWF are larger than the others from the TFs in the SWIM. This fact may be explained by the larger displaced area by this scenario. Cape St. Vincent (Fig. 3.2) in the southwest of Portugal might act as an obstacle to the tsunami leading to reduce the impact. The CWF has higher impact in the southern part of the study area but with decreasing inundation and amplitudes towards the north. Nevertheless, wave amplitudes of 5m cause considerable inundation in the northern part of the port. The waves produced

by CWF reach Sines 38 minutes after the earthquake (Table 3.2). The Gloria fault located at 37°N between 14°W and 24°W produces the smallest inundation in the study area. It is a transform fault triggering slight vertical movement because of 160° rake with a slip of 11m (Table 3.2). The scenario produces amplitudes between 0.3-0.4m with approximately 10 minute period (Fig. 3.6-b). The earthquake in 1941 generated similar waveforms showing weak attenuation with amplitudes around 0.4m in Cascais (Baptista et al., 1992; Baptista and Miranda, 2009). Site effects, observed in some few coastal locations (Fig. 3.6-a), caused MWH over 1m with some smaller inundation in unhabituated area between the container terminal and the intake and restitution points of the EDP power plant. Because of the larger distance to the Portuguese coast the tsunami travel time is approximately 85 minutes (Table 3.2).

The tide has important influence on tsunami impact in Sines. The tidal regime is semi-diurnal with an amplitude of about 2m. As expected the aggregate scenario at MHHW condition caused larger inundation areas and higher MFD values. On the other hand the aggregate scenario at MLLW produced larger drawback areas. A tsunami impact at low tide does not exclude the risk of heavy inundation and increases MDB by 16% compared to MHHW (Fig. 3.8).

We computed a map showing the contribution of the individual scenarios to the aggregated scenario at MSL (Fig. 3.9). Four scenarios contribute to the aggregate scenario, namely CWF, GBF, HSF and HSMPF. The main actor in the aggregated model is the HSMPF scenario that contributes with more than 60% independent of the tidal amplitude (Table 3.3). The scenarios CWF, GBF, HSF contribute about 12±4% to the aggregate model. The MPF and Gloria do not contribute to the aggregate scenario (Fig. 3.9).

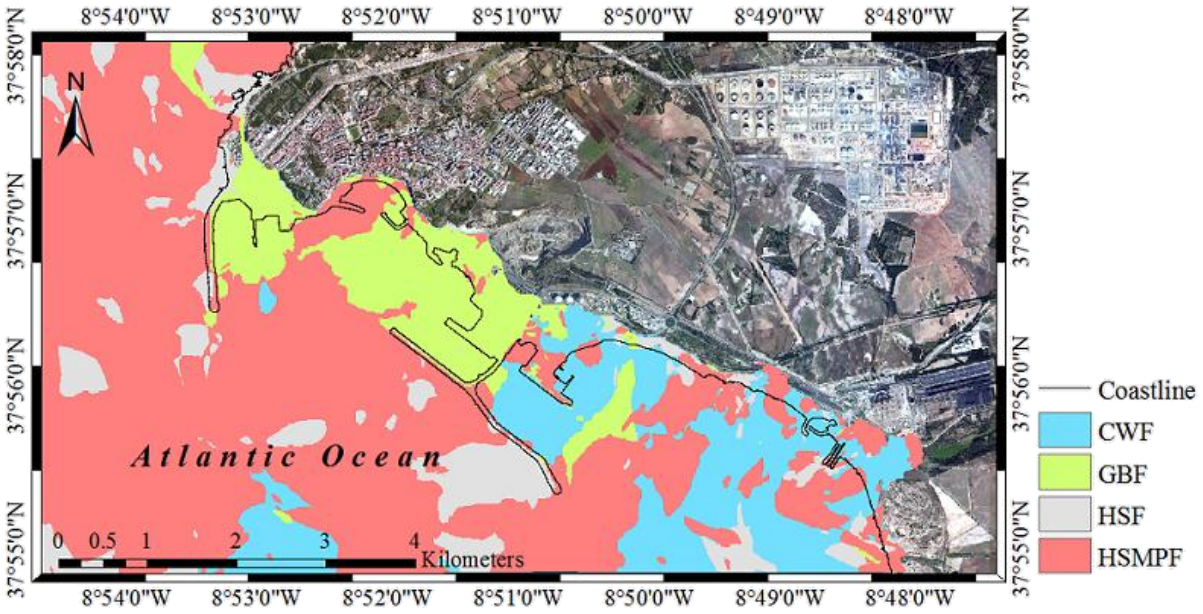

Figure 3.9 Contribution of individual scenarios to the aggregate model at MSL.

Table 3.3 Contribution of the scenarios to the aggregate model considering 3 stages of the tide.

Scenario	CWF [%]	GBF [%]	HSF [%]	HSMPF [%]
AGG MHHW	8.3	15.8	9.9	66
AGG MSL	15.1	12.4	10.0	62.5
AGG MLLW	16.8	11.7	11.1	60.3

Concluding we find that all SWIM scenarios (CWF, GBF, HSF, MPF and HSMPF) demonstrate high impact in Sines test site. Still the weakest source, the MPF, causes considerable inundation and MWH above 10m. The proximity of the faults within the SWIM results in short tsunami travel times. For the models MPF and HSMPF we calculated 22 minutes propagation time from the source to Sines test site. This closeness to possible tsunami sources raise the need of an efficient early warning system and meticulously planned evacuation for the port and other coastal areas. Also, coastal societies need to be educated and prepared for possible tsunami impact.

The Gloria fault differs from the other scenarios and produces MWH of approximately 1m in certain areas, one order of magnitude less than the scenarios in the SWIM.

The aggregate scenario allows to consider a set of faults to produce a synthesis of different scenarios. We further state the importance of this tool as important indicator for evacuation and city planners. We showed with the contribution map that different sources play varying importance in our study area. Although the worst case scenario may contribute more to the aggregate scenario than other considered faults, still other faults may have more significant impact on other parts of the test-site. The aggregate scenario is a valuable tool. Especially in areas exposed to threat from near-field sources, the aggregate scenario maps helps establishing accurate evacuation plans and thus allowing efficient and faster reaction to tsunami warning.

Acknowledgements

This work is funded by ASTARTE - Assessment, Strategy And Risk Reduction for Tsunamis in Europe - FP7- ENV2013 6.4-3, Grant 603839. The authors wish to thank Commandant José Brazuna Fontes of Sines harbour for his support for the field survey and Direção Geral do Território for making available LIDAR data of the study area. Finally, the authors wish to thank the reviewers for their suggestions that greatly improved the paper.

References

Antunes C.: Tabelas de Máximos, Médias e Mínimos. [online] Available at: <http://webpages.fc.ul.pt/~cmantunes/hidrografia/hidro_tabelas.html> [accessed 18th November 2014], 2014.

Atillah, A., El Hadani, D., Moudni, H., Lesne, O., Renou, C., Mangin, A. and Rouffi, F.: Tsunami vulnerability and damage assessment in the coastal area of Rabat and Salé, Morocco. Natural Hazards and Earth System Sciences, 11, 3397-3414., 2011.

Baptista, M. A., Miranda, P. and Victor, L. M.: Maximum entropy analysis of Portuguese tsunami data; the tsunamis of 28.02. 1969 and 26.05. 1975. Sci. Tsunami Hazards, 10(1), 9-20, 1992.

Baptista, M. A., Miranda, P. M. A., Miranda, J. M. and Victor, L. M.: Constrains on the source of the 1755 Lisbon tsunami inferred from numerical modelling of historical data on the source of the 1755 Lisbon tsunami. Journal of Geodynamics, 25(1), 159-174, 1998.

Baptista, M. A. and Miranda, J. M.: Revision of the Portuguese catalog of tsunamis. Natural Hazards and Earth System Science, 9(1), 25-42, 2009.

Baptista, M. A., Miranda, J. M., Omira, R. and Antunes, C.: Potential inundation of Lisbon downtown by a 1755-like tsunami. Natural Hazards and Earth System Science, 11(12), 3319-3326, 2011a.

Baptista, M. A., Miranda, J. M., Batllo, J. and Macia, R.: North East Atlantic Tsunamis Related with Gloria Fault. AGU Fall Meeting Abstracts, 2011b.

Benchekroun, S., Omira, R., Baptista, M. A., El Mouraouah, A., Brahim, A. I. and Toto, E. A.: Tsunami impact and vulnerability in the harbour area of Tangier, Morocco. Geomatics, Natural Hazards and Risk, (ahead-of-print), 1-23, 2013.

Câmara Municipal de Sines: Munícipio de Sines. [online] Available at: <http://www.sines.pt/PT/Negocios/potencialidades/turismo/Paginas/default.aspx> [accessed 18th September 2014], 2007 (in Portuguese)

Debrach, J. Raz de marée d'origine sismique eneregistrée sur le litoral Atlantique du Maroc, Service de Physique du Globe et de Meteorologie, Annales. Maroc ,1946 (in French).

Direção-geral do Território: LIDAR2011. Topographic and Bathymetric Information of Portuguese coastline, 2013.

Fukao, Y.: Thrust faulting at a lithospheric plate boundary the Portugal earthquake of 1969. Earth and Planetary Science Letters, 18(2), 205-216, 1973.

GEBCO: The General Bathymetric Chart of the Oceans, GEBCO_2014 Grid, version 20150318. [online] Available at: <http://www.gebco.net> [accessed July 2014], 2014.

Gràcia, E., Dañobeitia, J., Vergés, J., and PARSIFAL Team.: Mapping active faults offshore Portugal (36 N–38 N): implications for seismic hazard assessment along the southwest Iberian margin. Geology, 31(1), 83-86, 2003.

Grimison, N. L. and Chen, W. P.: The Azores-Gibraltar plate boundary: Focal mechanisms, depths of earthquakes, and their tectonic implications. Journal of Geophysical Research: Solid Earth (1978–2012), 91(B2), 2029-2047, 1986.

Gutenberg, B. and Richter, C. F.: Seismicity of the Earth and associated phenomena. Princeton University Press, New Jersey, 1949.

Gutscher, M. A., Malod, J., Rehault, J. P., Contrucci, I., Klingelhoefer, F., Mendes-Victor, L., and Spakman, W.: Evidence for active subduction beneath Gibraltar. Geology, 30(12), 1071-1074, 2002.

Instituto Hidrográfico de Portugal: Aproximações a Sines. Plano de Porto de Sines n° 26408. 3rd Edition. Marinha, Instituto Hidrográfico. Lisbon, 2010.

Instituto Hidrográfico de Portugal: Bathymetric Model of Sines. Modelo Batimetrico de Sines. [online] Available at: <http://www.hidrografico.pt/download-gratuito.php> [accessed 4th April 2014], 2012.

Instituto Nacional de Estatística: Census 2011. [online] Available at: <http://censos.ine.pt/xportal/xmain?xpid=CENSOS&xpgid=censos2011_apresentacao> [accessed 18th September 2014], 2011.

Johnston, A. C.: Seismic moment assessment of earthquakes in stable continental regions—III. New Madrid 1811–1812, Charleston 1886 and Lisbon 1755. Geophysical Journal International, 126(2), 314-344, 1996.

Kaabouben, F., Baptista, M. A., Iben Brahim, A., Mouraouah, A. E. and Toto, A.: On the moroccan tsunami catalogue. Natural Hazards and Earth System Science, 9(4), 1227-1236, 2009.

Laughton, A. S. and Whitmarsh, R. B.: The Azores-Gibraltar plate boundary. In Geodynamics of Iceland and the North Atlantic area (pp. 63-81). Springer Netherlands, 1974.

Lemos, C. R., Omira, R., Pinheiro, L. M., Baptista, M. A., Quaresma, L. S. And Garrido, C.: Tsunami Impact from a 1755-like event in the Aveiro Region, Portugal. In EGU General Assembly Conference Abstracts (Vol. 16, p. 15629), 2014.

Lima, V. V., Miranda, J. M., Baptista, M. A., Catalão, J., González Rodríguez, E. M., Otero, L. ... and Carreño Herrero, E.: Impact of a 1755-like tsunami in Huelva, Spain, 2010.

Liu, P. L. F., Cho, Y. S., Briggs, M. J., Kanoglu, U. and Synolakis, C. E.: Runup of solitary waves on a circular island. Journal of Fluid Mechanics, 302, 259-285, 1995.

Luis, J. F. Mirone: A multi-purpose tool for exploring grid data. Computers & Geosciences, 33(1), 31-41, 2007.

Luque, L., Lario, J., Zazo, C., Goy, J. L., Dabrio, C. J. and Silva, P. G.: Tsunami deposits as paleoseismic indicators: examples from the Spanish coast. Acta geológica hispánica, 36(3), 197-211, 2001.

Lynnes, C. S. and Ruff, L. J.: Source process and tectonic implications of the great 1975 North Atlantic earthquake. Geophysical Journal International, 82(3), 497-510, 1985.

Martins, I., and Mendes-Víctor, L. A.: Contribuição para o estudo da sismicidade de Portugal Continental. Universidade de Lisboa, Instituto Geofísico do Infante D. Luís, 1990, (in Portuguese).

Mendonça, J. M.: História Universal dos Terramotos que tem havido no mundo desde que ha noticia, desde a sua criação até ao século presente. Arq Nac da Torre de Tombo, Lisboa–Portugal, 1758(in Portuguese)

Miranda, J. M., Baptista, M. A., Terrinha, P. and Matias, L.: Tsunamigenic source areas for Portugal mainland, Iberia, Oral Communication, Session on Tsunami Early Warning Systems and Tsunami Risk Mitigation in the European-Mediterranean Region, 31st General Assembly of the European Seismological Commission, Crete, Greece, 2008.

Miranda, J. M., Luis, J. F., Reis, C., Omira, R., and Baptista, M. A.: Validation of NSWING, a multi-core finite difference code for tsunami propagation and run-up, American Geophysical Union (AGU) Fall Meeting, San Francisco. Paper Number: S21A-4390. Session Number and Title: S21A, Natural Hazards, 2014.

Okada, Y.: Surface deformation due to shear and tensile faults in a half-space. Bulletin of the seismological society of America, 75(4), 1135-1154, 1985.

Omira R., Baptista M. A., Matias L., Miranda J. M., Catita C., Carrilho F., and Toto E.: Design of a Sea-level Tsunami Detection Network for the Gulf of Cadiz. Nat Natural Hazards and earth System Science, 9:1327-1338, 2009.

Omira, R., Baptista, M. A., Miranda, J. M., Toto, E., Catita, C. and Catalao, J.: Tsunami vulnerability assessment of Casablanca-Morocco using numerical modelling and GIS tools. Natural hazards, 54(1), 75-95, 2010.

Omira, R., Baptista, M. A. and Miranda, J. M.: Evaluating tsunami impact on the Gulf of Cadiz coast (Northeast Atlantic). Pure and applied geophysics, 168(6-7), 1033-1043, 2011.

Omira, R., Baptista, M. A., Leone, F., Matias, L., Mellas, S., Zourarah, B. ... and Cherel, J. P.: Performance of coastal sea-defense infrastructure at El Jadida (Morocco) against tsunami threat: lessons learned from the Japanese 11 March 2011 tsunami. Natural Hazards and Earth System Sciences, 13, 1779-1794, 2013.

Omira, R., Baptista, M. A. and Matias, L.: Probabilistic Tsunami Hazard in the North East Atlantic from Near- and Far-field Tectonic Source. Pure App. Geophys., 172(3-4): 901-920, 2015.

Porto de Sines: Administração dos portos de Sines e do Algarve S.A. [online] Available at: <http://www.portodesines.pt/pls/portal/go> [accessed 18th September 2014], 2014.

Renou, C., Lesne, O., Mangin, A., Rouffi, F., Atillah, A., El Hadani, D. and Moudni, H.: Tsunami hazard assessment in the coastal area of Rabat and Salé, Morocco. Natural Hazards and Earth System Sciences, 11, 2181-2191, 2011.

Ribeiro, A., Mendes-Victor, L., Cabral, J. M. L. C., Matias, L., and Terrinha, P.: The 1755 Lisbon earthquake and the beginning of closure of the Atlantic. European Review, 14(02), 193-205, 2006.

Solares, J. M., and Arroyo, A. L.: The great historical 1755 earthquake. Effects and damage in Spain. Journal of Seismology, 8(2), 275-294, 2004.

Tinti, S., Tonini, R., Bressan, L., Armigliato, A., Gardi, A., Guillande, R. ... and Scheer, S.: Handbook of tsunami hazard and damage scenarios. JRC scientific and technical reports. EUR, 24691, 2011.

Zitellini, N., Chierici, F., Sartori, R. and Torelli, L.: The tectonic source of the 1755 Lisbon earthquake and tsunami. Annals of Geophysics, 42(1), 1999.

Zitellini, N., Mendes, L. A., Cordoba, D., Danobeitia, J., Nicolich, R., Pellis, G. ... and Ruiz, A. Z.: Source of 1755 Lisbon earthquake and tsunami investigated. Eos, Transactions American Geophysical Union, 82(26), 285-291, 2001.

Zitellini, N., Gràcia, E., Matias, L., Terrinha, P., Abreu, M. A., DeAlteriis, G. ... and Diez, S.: The quest for the Africa–Eurasia plate boundary west of the Strait of Gibraltar. Earth and Planetary Science Letters, 280(1), 13-50, 2009.

4. Discussion

The DTHA method was successfully applied to the study area in Sines. In the framework of ASTRATE I ran a total of eighteen scenarios using six typical faults associated with; CWF, GBF, HSF, MPF, HSMPF and Gloria for three stages of the tide (MLLW, MSL and MHHW). The results presented consist of integrated hazard maps for each scenario in MSL conditions and for the aggregate scenario (Fig. 3.4, 3.6 and 3.7). The influence of the tide in respect with the maximum inundation area and the maximum sea withdrawal is shown and I compared the impact of the aggregate scenario for three tide conditions (Fig. 3.8). In figure 3.9 the contribution to MWH offshore and MFD on land of each single scenario to the aggregate scenarios is presented. The results show that the composite fault HSMPF corresponds to worst case scenario in terms of tsunami impact.

The analysis of the synthetic waveforms confirms three different types of faults:

1.) The Gloria fault as a transform fault produces the weakest impact and a tsunami travel time of 85 min at the test site.

2.) The typical thrust faults GBF, MPF and HSF generating heavy impact, short tsunami travel times (22 min in case of MPF, 25 min in case of GBF and 30 min in HSF)

3.) Subduction slab with bigger rupture area producing higher periods and severe impact in Sines with 38 min tsunami travel time.

All faults located in the SWIM produce heavy impact scenarios when considering the MCE scenario. The tsunami arrival time is less than 40 minutes for all SWIM scenarios. The GF causes inundation at the beaches but leaves the harbour area dry even in MHHW conditions.

In consideration of the DTHA the discussion must be approached from a different point of view. In the papers by Tinti et al. (2011) the DTHA is considered as indispensable tool for tsunami mitigation measures and for tsunami warning systems. This approach has been successfully applied for tsunami hazard assessment, vulnerability analysis for specific locations around the world and along the Portuguese, Spanish and Moroccan coastline.

The quest of the 1755 Lisbon earthquake location and the high seismicity in the region favoured the intense investigations in the SWIM. The studies published in the last decades revealed successively more information and details of the study area. Bathymetric studies delivered details about the SWIMs morphology. Upon that seismic reflection and tomography allowed to obtain knowledge about the TFs and their potential in SWIM. This successive investigation led from a diffuse view to a clearer picture of SWIM. Nowadays thanks to these intense investigation the parameters of the TFs are well defined. This unequivocal physical definition of the TFs is a clear advantage for the DTHA.

This work presents an application of DTHA methodology to Sines. The study area contains numerous critical and fragile infrastructure. The application of DTHA delivers important information for municipality and port authorities about the tsunami impact. MFD values and inundation area describe which part on land will be affected in height and extension. MDB values show the maximum sea withdrawal. Subsequently mitigation measures must be established to reduce loss of life and property and damage in case of impact.

The DTHA is not the only Tsunami Hazard Assessment approach. The Probabilistic Tsunami Hazard Assessment (PTHA) employs large data bases considering a large number of possible scenarios and their corresponding recurrence rates. In case of PTHA studies the longer geological evidences reach back the more confidently can be calculated recurrence rates. Omira et al. (2015) published a probabilistic tsunami hazard assessment for the entire North East Atlantic. However, probabilistic studies should be interpreted carefully and must not be considered to establish mitigation measures. For the mitigation measures and coastal engineering the DTHA is more appropriate as the MCE scenarios are considered. Results are easier to interpret and deliver clear limits of maximum inundation area and values of MFD. A comprehensive study should include both methods DTHA and PTHA presenting both worst case and exceeding maximum wave heights with likelihood estimations.

DTHA has inherent limitations. The initial condition of the tsunami model, initial sea surface elevation the limitations of the simulation model and the DEM. To calculate the initial condition the model used

considers the fault area to be rectangular. Although this is nearly never the case, this approximation is considered valid as considered fault areas are usually big (hundreds of square kilometres) and can be reduced to simpler geometry. The initial condition is calculated on base of the elastic half space theory (Okada, 1985). The parameters used are estimated upon geological constraints obtained from recent year's investigation.

Another limitation of the model used is the assumption of instantaneous rupture mechanism neglecting the dynamic of the seabed deformation. This approximation is limited in case of slow rupture velocities and tsunami earthquakes or large fault dimensions when considering mega thrust faults. However, in the SWIM where common thrust faults and subduction zone earthquakes are dominant this assumption is valid.

Tsunami propagation was calculated using the NSWING model based on the non-linear shallow water equations. This model solves the Navier-Stokes equations for water wave propagation using the approximation that vertical velocity components of water particles is negligible and horizontal motion is uniform in the entire water column of the fluid (Tinti et al. 2011). Further the ocean is considered as incompressible fluid and the initial condition is transferred to the sea surface. This assumption is valid if the wave length is much greater than the water depth. The model includes bottom friction terms but the Manning roughness coefficient is set to zero as worst case tsunami has been assumed. When computing worst case tsunami scenarios it is a common procedure to set Manning roughness coefficient to zero to obtain unambiguous areas of inundation (Omira et al., 2010). The non-linear SWEs on the other hand do not include frequency dispersion terms. Their importance is discussed in literature and frequency dispersion is assumed to play an important role for transoceanic tsunami propagation. In this study this is not the case as all TFs are local or regional sources. Tsunami travel times are about half an hour for the SWIM scenarios and one and a half hour for the Gloria fault.

The DEM used has a resolution of 10m. Main coastal defence structures are implemented in the model. Generally spoken finer resolution of the DEM leads to more detailed results. However, this is often a difficult task as high resolution data in near shore areas is often not available. The recent published LIDAR data set with 2m resolution (Direção-Geral do Território, 2013) enables the computation of accurate DEMs. In spite of the high resolution on land and in the near shore areas covered the LIDAR data set the connecting data sets (nautical charts and bathymetric) provide less information. In this areas along the continental shelf higher resolution data is desirable. However, the DEM used in the study presents best compromise based on most actual available data sets. Main coastal defence structures and all important geological features are represented by the DEM.

DTHA is applied on small study areas commonly with major socio-economic interest, but still many locations are left without DTHA and consequential mitigation measures. In the Gulf of Cadiz area there specific studies applying DTHA. However, there are still many areas without appropriate tsunami hazard assessment confirming the need for more studies of DTHA along bordering coastlines. But additionally it is important to subsequently realize the right measurements to reduce impact.

For those study areas where DTHA has been applied only little mitigation measures have been carried out so far. Still no suitable evacuation routes or clear classified tsunami-safe areas have been presented. No signs have been placed indicating how to react at popular beaches, nor signs indicating tsunami evacuation routes. No specific tsunami training has been prepared for coastal communities. People are left uninformed what to do in case of a tsunami. It is not the goal to apply a number DTHAs and leave the results to a small specialized scientific community. Therefor an international standardized procedure is useful for authorities to establish mitigation measures. Up to now many efforts have been carried out to implement tsunami warning systems in the Northeast Atlantic, Mediterranean and connecting seas and many of them are operational already. However, waring is based on decision matrices in the North East Atlantic which has some operational delay. This delay might be crucial for sites closer to the earthquake. Mitigations measures like drills and exercises must be carried out by officials to prepare communities for self-evacuation. The reduced death toll in the recent 16th September 2015 Chile earthquake goes back to consequent warning and self-evacuation.

Consequences due to unpreparedness may be fatal as learnt from the India Ocean Tsunami 2004. The focus must be on successive and consequent tsunami hazard assessment in all prone coastal areas.

Tsunami secure zones must be identified and indicated. Evacuation routes from impact areas must be established and signposted. Additionally civil protection, coast guard, maritime police, fire brigades and coastal communities must be informed and trained how to react. The overall goal must be to create tsunami resilient and tsunami ready societies in potential risk areas.

To sum up, the DTHA is based upon certain approximation that deliver best possible solutions if chosen correctly. In more specific cases one should take into account the limitations existing in the methodology. In this study the DTHA approach shows heavy impact for all SWIM scenarios. It is suggested to begin immediately to establish evacuation plans especially for the port area and the beaches and prepare a tsunami resilient society in Sines.

5. Conclusion

In this master thesis the goal was to apply a Deterministic Tsunami Hazard Assessment (DTHA) on the test site in Sines, Portugal. The DTHA consists in studying the sources; choosing the tsunami scenarios; computing the initial condition; Preparation of the DEM and the set of computational grids; computation of the numerical models and analysis and interpretation of the results. All these steps were carried out successfully.

The results of the DTHA in Sines confirm that all local sources have heavy impacts in the test site. The weakest scenario in the SWIM is the MPF scenario with a maximum wave height of 10m. The composite source HSMPF is the worst case scenario and contributes with more than 60% at all stages of the tide to the aggregate scenario. An aggregate scenarios has been built synthesizing the effect of all possible MCE scenarios. A clear influence of the tide could be shown. Under unfavourable conditions with high tide a tsunami impact affects bigger areas in Sines. The tsunami travel time for the sources in the SWIM is less than 30 min accept for the CWF. This fact and the heavy impact of all local sources make the aggregate scenario a valuable output for authorities and city planners. The regional scenario GF shows the weakest impact inundating only parts of the beaches. With the DTHA, worst case tsunami scenarios can be modelled giving the most important parameter to describe the impact at the test-site. These results however do not represent probabilities of a tsunami impact. In an ideal case the DTHA can be complemented with a Probabilistic Tsunami Hazard Assessment (PTHA). Omira et al. (2015) complete the results found in this thesis using PTHA in the same test site.

The DTHA is the only method that produces easy to interpret results that can be immediately used for profound mitigation measures. The limitations of the approach must be considered and justified throughout the proceeding, to convey best possible and doubtless results. By defining an international standardized procedure for this approach could help to make it easier to use, to interpret and to establish mitigation measures. Future investigation on the numerical models making them more efficient and exact may play a key role for tsunami warning systems. If the rupture mechanism of a submarine earthquake are identified rapidly DTHA analyses will enable scientists to elaborate tsunami hazard maps before impact. Nevertheless society must be trained and models prepared. But when considering local sources efficient mitigation measures are indispensable.

6. References

Aki, K. (1972). Earthquake mechanism. Tectonophysics, 13(1), 423-446.

Antunes C. (2014). Tabelas de Máximos, Médias e Mínimos. [online] Available at: <http://webpages.fc.ul.pt/~cmantunes/hidrografia/hidro_tabelas.html> [accessed 18th November 2014].

Atillah, A., El Hadani, D., Moudni, H., Lesne, O., Renou, C., Mangin, A. and Rouffi, F. (2011). Tsunami vulnerability and damage assessment in the coastal area of Rabat and Salé, Morocco. Natural Hazards and Earth System Sciences, 11, 3397-3414.

Baptista, M. A., Miranda, P. and Victor, L. M. (1992). Maximum entropy analysis of Portuguese tsunami data; the tsunamis of 28.02. 1969 and 26.05. 1975. Sci. Tsunami Hazards, 10(1), 9-20.

Baptista, M. A., Heitor, S., Miranda, J. M., Miranda, P. and Victor, L. M. (1998a). The 1755 Lisbon tsunami; evaluation of the tsunami parameters. *Journal of Geodynamics*, *25*(1), 143-157.

Baptista, M. A., Miranda, P. M. A., Miranda, J. M. and Victor, L. M. (1998b). Constrains on the source of the 1755 Lisbon tsunami inferred from numerical modelling of historical data on the source of the 1755 Lisbon tsunami. *Journal of Geodynamics*, *25*(1), 159-174.

Baptista, M. A. and Miranda, J. M. (2009). Revision of the Portuguese catalog of tsunamis. Natural Hazards and Earth System Science, 9(1), 25-42.

Baptista, M. A., Miranda, J. M., Omira, R. and Antunes, C. (2011a). Potential inundation of Lisbon downtown by a 1755-like tsunami. Natural Hazards and Earth System Science, 11(12), 3319-3326.

Baptista, M. A., Miranda, J. M., Batllo, J. and Macia, R. (2011b). North East Atlantic Tsunamis Related with Gloria Fault. AGU Fall Meeting Abstracts.

Benchekroun, S., Omira, R., Baptista, M. A., El Mouraouah, A., Brahim, A. I. and Toto, E. A. (2013). Tsunami impact and vulnerability in the harbour area of Tangier, Morocco. Geomatics, Natural Hazards and Risk, (ahead-of-print), 1-23.

Bowden, K.F. (1983). Physical Oceanography of Coastal Waters. *Ellis Horwood Ltd., New York*. 302 pp.

Bryant, E. (2014). *Tsunami: the underrated hazard*. Springer.

Câmara Municipal de Sines (2007). Munícipio de Sines. [online] Available at: <http://www.sines.pt/PT/Negocios/potencialidades/turismo/Paginas/default.aspx> [accessed 18th September 2014], (in Portuguese).

Cunha, T. A., Matias, L. M., Terrinha, P., Negredo, A. M., Rosas, F., Fernandes, R. M. S. and Pinheiro, L. M. (2012). Neotectonics of the SW Iberia margin, Gulf of Cadiz and Alboran Sea: a reassessment including recent structural, seismic and geodetic data. *Geophysical Journal International*, *188*(3), 850-872.

Debrach, J. (1946). Raz de marée d'origine sismique eneregistrée sur le litoral Atlantique du Maroc, Service de Physique du Globe et de Meteorologie, Annales. Maroc. (in French).

de Sousa, F. L. P. (1919). *O terremoto do 1.0 de Novembro de 1755 em Portugal e um estudo demografico* (Vol. 1). Tip. do Comercio.

Direção-geral do Território (2013). LIDAR2011. Topographic and Bathymetric Information of Portuguese coastline.

Duarte, J. C., Rosas, F. M., Terrinha, P., Schellart, W. P., Boutelier, D., Gutscher, M. A. and Ribeiro, A. (2013). Are subduction zones invading the Atlantic? Evidence from the southwest Iberia margin. *Geology*, *41*(8), 839-842.

Dutykh, D. and Dias, F. (2007). Water waves generated by a moving bottom. In *Tsunami and Nonlinear waves* (pp. 65-95). Springer Berlin Heidelberg.

Dutykh, D. (2008). Mathematical modeling of tsunamis. PhD thesis, pp. 256, Ecole Normal Superieur de Cachan, France.

Fernandes, R. M. S., Ambrosius, B. A. C., Noomen, R., Bastos, L., Wortel, M. J. R., Spakman, W. and Govers, R. (2003). The relative motion between Africa and Eurasia as derived from ITRF2000 and GPS data. *Geophysical Research Letters*, *30*(16).

Fukao, Y. (1973). Thrust faulting at a lithospheric plate boundary the Portugal earthquake of 1969. *Earth and Planetary Science Letters*, *18*(2), 205-216.

GEBCO (2014). The General Bathymetric Chart of the Oceans, GEBCO_2014 Grid, version 20150318. [online] Available at: <http://www.gebco.net> [accessed July 2014].

González, A., Torné, M., Córdoba, D., Vidal, N., Matias, L. M. and Díaz, J. (1996). Crustal thinning in the southwestern Iberia margin. *Geophysical Research Letters*, *23*(18), 2477-2480.

Gràcia, E., Dañobeitia, J., Vergés, J. and PARSIFAL Team. (2003). Mapping active faults offshore Portugal (36 N–38 N): implications for seismic hazard assessment along the southwest Iberian margin. *Geology*, *31*(1), 83-86.

Grilli, S. T., Taylor, O. D. S., Baxter, C. D. and Maretzki, S. (2009). A probabilistic approach for determining submarine landslide tsunami hazard along the upper east coast of the United States. *Marine Geology*, *264*(1), 74-97.

Grimison, N. L. and Chen, W. P. (1986). The Azores-Gibraltar plate boundary: Focal mechanisms, depths of earthquakes, and their tectonic implications. Journal of Geophysical Research: Solid Earth (1978–2012), 91(B2), 2029-2047.

Gupta, H. K. and Gahalaut, V. K. (2013). Three Great Tsunamis: Lisbon (1755), Sumatra-Andaman (2004) and Japan (2011). Springer.

Gutenberg, B. and Richter, C. F. (1949). Seismicity of the Earth and associated phenomena. Princeton University Press, New Jersey.

Gutscher, M. A., Malod, J., Rehault, J. P., Contrucci, I., Klingelhoefer, F., Mendes-Victor, L. and Spakman, W. (2002). Evidence for active subduction beneath Gibraltar. *Geology*, *30*(12), 1071-1074.

Gutscher, M. A., Dominguez, S., Westbrook, G. K., Le Roy, P., Rosas, F., Duarte, J. C. ... and Bartolomé, R. (2012). The Gibraltar subduction: A decade of new geophysical data. *Tectonophysics*, *574*, 72-91.

Hayward, N., Watts, A. B., Westbrook, G. K., & Collier, J. S. (1999). A seismic reflection and GLORIA study of compressional deformation in the Gorringe Bank region, eastern North Atlantic. *Geophysical Journal International*, *138*(3), 831-850.

Helene, O. and Yamashita, M. T. (2006). Understanding the tsunami with a simple model. *European journal of physics*, *27*(4), 855.

Imamura, F. (1995). Review of tsunami simulation with a finite difference method, Long-wave runup models. World Scientific, 25–42.

Instituto Hidrográfico de Portugal (2010). Aproximações a Sines. Plano de Porto de Sines n° 26408. 3rd Edition. Marinha, Instituto Hidrográfico. Lisbon.

Instituto Hidrográfico de Portugal (2012). Bathymetric Model of Sines. Modelo Batimetrico de Sines. [online] Available at: <http://www.hidrografico.pt/download-gratuito.php> [accessed 4th April 2014].

Instituto Nacional de Estatística (2011). Census 2011. [online] Available at: <http://censos.ine.pt/xportal/xmain?xpid=CENSOS&xpgid=censos2011_apresentacao> [accessed 18th September 2014].

Intergovernmental Oceanographic Commission (2013). Revised Edition 2013. Tsunami Glossary, 2013.

Istituto Nazionale di Geofisica e Vulcanologia (2015). Individual Seismogenic Sources. [online] <http://diss.rm.ingv.it/diss/index.php/tutorial/15-individual-seismogenic-sources> Available at: [accessed 9th September 2015].

Johnston, A. C. (1996). Seismic moment assessment of earthquakes in stable continental regions—III. New Madrid 1811–1812, Charleston 1886 and Lisbon 1755. *Geophysical Journal International*, *126*(2), 314-344.

Kaabouben, F., Baptista, M. A., Iben Brahim, A., Mouraouah, A. E. and Toto, A. (2009). On the moroccan tsunami catalogue. *Natural Hazards and Earth System Science*, *9*(4), 1227-1236.

Kanamori, H. (1972). Mechanism of tsunami earthquakes. *Physics of the earth and planetary interiors*, *6*(5), 346-359.

Kanamori, H. (1977). The energy release in great earthquakes. *Journal of geophysical research*, *82*(20), 2981-2987.

Kajiura, K. (1970). 45. Tsunami Source, Energy and the Directivity of Wave Radiation.

Laughton, A. S. and Whitmarsh, R. B. (1974). The Azores-Gibraltar plate boundary. In Geodynamics of Iceland and the North Atlantic area (pp. 63-81). Springer Netherlands.

Lemos, C. R., Omira, R., Pinheiro, L. M., Baptista, M. A., Quaresma, L. S. and Garrido, C. (2014). Tsunami Impact from a 1755-like event in the Aveiro Region, Portugal. In *EGU General Assembly Conference Abstracts* (Vol. 16, p. 15629).

Lima, V. V., Miranda, J. M., Baptista, M. A., Catalão, J., González Rodríguez, E. M., Otero, L. ... and Carreño Herrero, E. (2010). Impact of a 1755-like tsunami in Huelva, Spain.

Linsley, R.K. and Franzini, J.B. (1979). Water Resources Engineering. 3rd Edition. *McGraw-Hill Book Co.*, New York, pp 125–126.

Liu, P. L. F., Cho, Y. S., Briggs, M. J., Kanoglu, U. and Synolakis, C. E. (1995). Runup of solitary waves on a circular island. *Journal of Fluid Mechanics*, *302*, 259-285.

Liu, P. L. F., Woo, S. B., Cho, Y. S. (1998). Computer programs for tsunami propagation and inundation. Technical report, Cornell University.

Luis, J. F. (2007). Mirone: A multi-purpose tool for exploring grid data. *Computers & Geosciences*, *33*(1), 31-41.

Luque, L., Lario, J., Zazo, C., Goy, J. L., Dabrio, C. J. and Silva, P. G. (2001). Tsunami deposits as paleoseismic indicators: examples from the Spanish coast. *Acta geológica hispánica*, *36*(3), 197-211.

Lynnes, C. S. and Ruff, L. J. (1985). Source process and tectonic implications of the great 1975 North Atlantic earthquake. *Geophysical Journal International*, *82*(3), 497-510.

Mansinha, L. and Smylie, D. E. (1971). The Displacement Field of Inclined Faults. Bull. Seismol. Soc. Am. 61(5): 1433–1440.

Martínez-Loriente, S., Gràcia, E., Bartolome, R., Sallarès, V., Connors, C., Perea, H. ... and Zitellini, N. (2013). Active deformation in old oceanic lithosphere and significance for earthquake hazard: Seismic imaging of the Coral Patch Ridge area and neighboring abyssal plains (SW Iberian Margin). *Geochemistry, Geophysics, Geosystems*, *14*(7), 2206-2231.

Martínez-Loriente, S., Sallarès, V., Gràcia, E., Bartolome, R., Dañobeitia, J. J. and Zitellini, N. (2014). Seismic and gravity constraints on the nature of the basement in the Africa-Eurasia plate boundary: New insights for the geodynamic evolution of the SW Iberian margin. *Journal of Geophysical Research: Solid Earth*, *119*(1), 127-149.

Martins, I. and Mendes-Víctor, L. A. (1990). Contribuição para o estudo da sismicidade de Portugal Continental. *Universidade de Lisboa, Instituto Geofísico do Infante D. Luís*, (1990), (in Portuguese).

Mendes-Victor, L., Oliveira, C. S., Azevedo, J. and Ribeiro, A. (Eds.). (2008). *The 1755 Lisbon earthquake: revisited* (Vol. 7). Springer Science & Business Media.

Matias, L. M., Cunha, T., Annunziato, A., Baptista, M. A. and Carrilho, F. (2013). Tsunamigenic earthquakes in the Gulf of Cadiz: fault model and recurrence. *Natural Hazards and Earth System Science*, *13*(1), 1-13.

McClusky, S., Reilinger, R., Mahmoud, S., Sari, D. B. and Tealeb, A. (2003). GPS constraints on Africa (Nubia) and Arabia plate motions. *Geophysical Journal International*, *155*(1), 126-138.

Mendonça, J. M. (1758). História Universal dos Terramotos que tem havido no mundo desde que ha noticia, desde a sua criação até ao século presente. *Arq Nac da Torre de Tombo, Lisboa–Portugal*, (in Portuguese).

Miranda, J. M., Baptista, M. A., Terrinha, P. and Matias, L. (2008). Tsunamigenic source areas for Portugal mainland, Iberia, Oral Communication, Session on Tsunami Early Warning Systems and Tsunami Risk Mitigation in the European-Mediterranean Region, 31st General Assembly of the European Seismological Commission, Crete, Greece.

Miranda, J. M., Luis, J. F., Reis, C., Omira, R., and Baptista, M. A. (2014). Validation of NSWING, a multi-core finite difference code for tsunami propagation and run-up, American Geophysical Union (AGU) Fall Meeting, San Francisco. Paper Number: S21A-4390. Session Number and Title: S21A, Natural Hazards.

Mitsoudis, D. A., Flouri, E. T., Chrysoulakis, N., Kamarianakis, Y., Okal, E. A., and Synolakis, C. E. (2012). Tsunami hazard in the southeast Aegean Sea. *Coastal Engineering*, *60*, 136-148.

Monna, S., Argnani, A., Cimini, G. B., Frugoni, F. and Montuori, C. (2015). Constraints on the geodynamic evolution of the Africa–Iberia plate margin across the Gibraltar Strait from seismic tomography. *Geoscience Frontiers*, *6*(1), 39-48.

Nocquet, J. M. and Calais, E. (2004). Geodetic measurements of crustal deformation in the Western Mediterranean and Europe. *Pure and Applied Geophysics*, *161*(3), 661-681.

Okada, Y. (1985). Surface deformation due to shear and tensile faults in a half-space. *Bulletin of the seismological society of America*, *75*(4), 1135-1154.

Omira R., Baptista M. A., Matias L., Miranda J. M., Catita C., Carrilho F., and Toto E. (2009). Design of a Sea-level Tsunami Detection Network for the Gulf of Cadiz. Nat *Natural Hazards and earth System Science,* 9:1327-1338.

Omira R. (2010). Modeling Tsunamis Impact in northwestern Morocco and southwestern Iberia. *PhD–Dissertation*. Ibn Tofail University. Morocco.

Omira, R., Baptista, M. A., Miranda, J. M., Toto, E., Catita, C. and Catalao, J. (2010). Tsunami vulnerability assessment of Casablanca-Morocco using numerical modelling and GIS tools. *Natural hazards*, *54*(1), 75-95.

Omira, R., Baptista, M. A. and Miranda, J. M. (2011). Evaluating tsunami impact on the Gulf of Cadiz coast (Northeast Atlantic). *Pure and applied geophysics*, *168*(6-7), 1033-1043.

Omira, R., Baptista, M. A., Leone, F., Matias, L., Mellas, S., Zourarah, B. ... and Cherel, J. P. (2013). Performance of coastal sea-defense infrastructure at El Jadida (Morocco) against tsunami threat: lessons learned from the Japanese 11 March 2011 tsunami. *Natural Hazards and Earth System Sciences*, *13*, 1779-1794.

Omira, R., Baptista, M. A., and Matias, L. (2015). Probabilistic Tsunami Hazard in the Northeast Atlantic from Near-and Far-Field Tectonic Sources. *Pure and Applied Geophysics*, *172*(3-4), 901-920.

Pedlosky, J. (2003). Waves in the ocean and atmosphere: introduction to wave dynamics. Springer Science & Business Media.

Phuong, N. H., Que, B. C., and Phuong, V. H. Pham The Truyen, (2014). Scenario-based tsunami hazard assessment for the coast of Vietnam from the Manila Trench source. *Physics of the Earth and Planetary Interiors*, *236*, 95-108.

Porto de Sines (2014). Administração dos portos de Sines e do Algarve S.A. [online] Available at: <http://www.portodesines.pt/pls/portal/go> [accessed 18th September 2014].

Renou, C., Lesne, O., Mangin, A., Rouffi, F., Atillah, A., El Hadani, D. and Moudni, H. (2011). Tsunami hazard assessment in the coastal area of Rabat and Salé, Morocco. *Natural Hazards and Earth System Sciences*, *11*, 2181-2191.

Ribeiro, A., Mendes-Victor, L., Cabral, J. M. L. C., Matias, L., and Terrinha, P. (2006). The 1755 Lisbon earthquake and the beginning of closure of the Atlantic. *European Review, 14(02)*, 193-205.

Rosas, F. M., Duarte, J. C., Neves, M. C., Terrinha, P., Silva, S., Matias, L. ... and Bartolomé, R. (2012). Thrust–wrench interference between major active faults in the Gulf of Cadiz (Africa–Eurasia plate boundary, offshore SW Iberia): Tectonic implications from coupled analog and numerical modeling. *Tectonophysics*, *548*, 1-21.

Sartori, R., Torelli, L., Zitellini, N., Peis, D. and Lodolo, E. (1994). Eastern segment of the Azores-Gibraltar line (central-eastern Atlantic): An oceanic plate boundary with diffuse compressional deformation. *Geology*, *22*(6), 555-558.

Sella, G. F., Dixon, T. H. and Mao, A. (2002). REVEL: A model for recent plate velocities from space geodesy. *Journal of Geophysical Research: Solid Earth (1978–2012)*, *107*(B4), ETG-11.

Solares, J. M., Arroyo, A. L. and Mezcua, J. (1979). Isoseismal map of the 1755 Lisbon earthquake obtained from Spanish data. *Tectonophysics*, *53*(3), 301-313.

Solares, J. M. and Arroyo, A. L. (2004). The great historical 1755 earthquake. Effects and damage in Spain. *Journal of Seismology*, *8*(2), 275-294.

Sorensen, R. M. (2006). Basic coastal engineering (Vol. 10). Springer Science & Business Media.

Sørensen, M. B., Spada, M., Babeyko, A., Wiemer, S. and Grünthal, G. (2012). Probabilistic tsunami hazard in the Mediterranean Sea. *Journal of Geophysical Research: Solid Earth (1978–2012)*, *117*(B1).

Synolakis, C. E. (2003). Tsunami and seiche. *Earthquake engineering handbook*, 9_1-9_90.

Synolakis, C. E. and Bernard, E. N. (2006). Tsunami science before and beyond Boxing Day 2004. *Philosophical Transactions of the Royal Society of London A: Mathematical, Physical and Engineering Sciences*, *364*(1845), 2231-2265.

Ten Brink, U. S., Barkan, R., Andrews, B. D. and Chaytor, J. D. (2009). Size distributions and failure initiation of submarine and subaerial landslides. *Earth and Planetary Science Letters*, *287*(1), 31-42.

Terrinha, P., Pinheiro, L. M., Henriet, J. P., Matias, L., Ivanov, M. K., Monteiro, J. H. ... and Rovere, M. (2003). Tsunamigenic-seismogenic structures, neotectonics, sedimentary processes and slope instability on the southwest Portuguese Margin. *Marine Geology*, *195*(1), 55-73.

Terrinha, P., Matias, L., Vicente, J., Duarte, J., Luis, J., Pinheiro, L. ... and MATESPRO Team. (2009). Morphotectonics and strain partitioning at the Iberia–Africa plate boundary from multibeam and seismic reflection data. *Marine Geology*, *267*(3), 156-174.

Tinti, S., Tonini, R., Bressan, L., Armigliato, A., Gardi, A., Guillande, R. ... and Scheer, S. (2011). Handbook of tsunami hazard and damage scenarios. *JRC scientific and technical reports. EUR*, *24691*.

Tinti, S., and Tonini, R. (2013). The UBO-TSUFD tsunami inundation model: validation and application to a tsunami case study focused on the city of Catania, Italy. *Natural Hazards and Earth System Sciences (NHESS)*.

Titov, V. V. and Synolakis, C. E. (1995). Modeling of breaking and non-breaking long-wave evolution and runup using VTCS-2. J. Waterway Port Ocean Coast. Eng. 121: 308–316.

Titov, V. V. and Synolakis, C. E. (1998). Numerical modeling of tidal wave runup. J. Waterway Port Ocean Coast. Eng. 124: 157–171.

Tonini, R., Armigliato, A., Pagnoni, G., Zaniboni, F. and Tinti, S. (2011). Tsunami hazard for the city of Catania, eastern Sicily, Italy, assessed by means of Worst-case Credible Tsunami Scenario Analysis (WCTSA). *Nat. Hazards Earth Syst. Sci*, *11*, 1217-1232.

Tortella, D., Torne, M. and Pérez-Estaún, A. (1997). Geodynamic evolution of the eastern segment of the Azores-Gibraltar zone: the Gorringe Bank and the Gulf of Cadiz region. *Marine Geophysical Researches*, *19*(3), 211-230.

Vallina, A. U. (1999). Principles of seismology. *Cambridge University Press*.

Wang, X. (2009). User manual for COMCOT version 1.7 (first draft). Cornel University, 65.

Wijetunge, J. J. (2014). A deterministic analysis of tsunami hazard and risk for the southwest coast of Sri Lanka. *Continental Shelf Research*, *79*, 23-35.

Zitellini, N., Chierici, F., Sartori, R. and Torelli, L. (1999). The tectonic source of the 1755 Lisbon earthquake and tsunami. *Annals of Geophysics*, *42*(1).

Zitellini, N., Mendes, L. A., Cordoba, D., Danobeitia, J., Nicolich, R., Pellis, G. ... and Ruiz, A. Z. (2001). Source of 1755 Lisbon earthquake and tsunami investigated. *Eos, Transactions American Geophysical Union*, *82*(26), 285-291.

Zitellini, N., Gràcia, E., Matias, L., Terrinha, P., Abreu, M. A., DeAlteriis, G. ... and Diez, S. (2009). The quest for the Africa–Eurasia plate boundary west of the Strait of Gibraltar. *Earth and Planetary Science Letters*, *280*(1), 13-50.